

Integrating brain and biomechanical models - a new paradigm for understanding neuro-muscular control

Sebastian S. James^{1,2}, Chris Papapavlou⁵, Alexander Blenkinsop^{1,2},
Alexander J. Cope³,

Sean Anderson^{2,4}, Konstantinos Moustakas⁵, Kevin N. Gurney^{1,2,*}

¹ Adaptive Behaviour Research Group, Department of Psychology, The University of Sheffield, Sheffield, UK

² Insigneo Institute for *in-silico* Medicine, The University of Sheffield, Sheffield, UK

³ Department of Computer Science, The University of Sheffield, Sheffield, UK

⁴ Department of Automatic Control Systems Engineering, The University of Sheffield, Sheffield, UK

⁵ Department of Electrical and Computer Engineering, The University of Patras, Patras, Greece

Correspondence*:

Kevin N. Gurney

Department of Psychology, The University of Sheffield, Western Bank, Sheffield, S10 2TP, UK, k.gurney@sheffield.ac.uk

2 ABSTRACT

To date, realistic models of how the central nervous system governs behaviour have been restricted in scope to the brain, brainstem or spinal column, as if these existed as disembodied organs. Further, the model is often exercised in relation to an *in vivo* physiological experiment with input comprising an impulse, a periodic signal or constant activation, and output as a pattern of neural activity in one or more neural populations. Any link to behaviour is inferred only indirectly via these activity patterns. We argue that to discover the principles of operation of neural systems, it is necessary to express their behaviour in terms of physical movements of a realistic motor system, and to supply inputs that mimic sensory experience. To do this with confidence, we must connect our brain models to neuro-muscular models and provide relevant visual and proprioceptive feedback signals, thereby closing the loop of the simulation. This paper describes an effort to develop just such an integrated brain and biomechanical system using a number of pre-existing models. It describes a model of the saccadic oculomotor system incorporating a neuromuscular model of the eye and its six extraocular muscles. The position of the eye determines how illumination of a retinotopic input population projects information about the location of a saccade target into the system. A pre-existing saccadic burst generator model was incorporated into the system, which generated motoneuron activity patterns suitable for driving the biomechanical eye. The model was demonstrated to make accurate saccades to a target luminance under a set of environmental constraints. Challenges encountered in the development of this model showed the importance of this integrated modelling approach. Thus, we exposed shortcomings in individual model components which were only apparent when these

were supplied with the more plausible inputs available in a closed loop design. Consequently we were able to suggest missing functionality which the system would require to reproduce more realistic behaviour. The construction of such closed-loop animal models constitutes a new paradigm of *computational neurobehaviour* and promises a more thoroughgoing approach to our understanding of the brain's function as a controller for movement and behaviour.

Keywords: integrated brain biomechanics neuromuscular neuromechanics oculomotor saccade basal-ganglia

1 INTRODUCTION

The field of computational neuroscience has provided many *systems models* of the brain (Arai et al., 1994; Gancarz and Grossberg, 1998; Hazy et al., 2007; Blenkinsop et al., 2017). We refer to these as *mechanistic computational models*, meaning models which consist of populations of neural elements, interconnected in a biologically plausible manner, which simulate the operation of the brain. Whilst they differ in scale and complexity, these models all seek to describe the fundamental mechanisms behind common animal behaviours such as locomotion, threat evasion, reaching or feeding. However, none of the models cited here actually reproduce these behaviours. In each case, the activity in a certain population of neurons is taken to be representative of a behavioural outcome. In some cases, it is reasonable to take the activity of an internal population within the brain model as being representative of the induced behaviour. For example, a choice made in a *go/no-go* task could be determined from activity in a population within a basal ganglia model (Nambu et al., 1990; Kühn et al., 2004). The decision to *go* is selected by a reduction of activity in this population; maintenance of activity implies *no-go*. To validate the model, the error rates which it generates could be compared with experimentally determined error rates in primate subjects. We refer to this as an *output assumption model* because the output is assumed to signify behaviour. (An *input assumption model* assumes that sensory input produces some particular form of neural activity in an input population of the model.)

However, we may be interested in reproducing accurate simulated *trajectories*, in order to find out how degradation of parts of the model affect movement. In Parkinson's Disease, degradation of the dopamine neurons originating in the substantia nigra pars compacta (SNc) causes dyskinesia (Galvan and Wichmann, 2008), as well as abnormal network activity in the basal ganglia (Brown et al., 2001; McCarthy et al., 2011). Sufferers of the disease would be expected to produce abnormal decision-making *and* movement trajectories in a reach-to-the-correct-target task such as the one described in James et al. (2017). A model which sought to explore in detail the effects of the SNc degradation both on the decision making *and* on the movement dynamics would need a physically accurate virtual arm, as well as physically realistic sensory input for the brain. This is no less than a complete model of those sections of the brain and body which act to fulfil the task. Such a modelling effort, if successful, would result in a virtual robot capable of expressing behaviour *in response to sensory input from its environment*. This would represent a paradigm shift in the field of computational neuroscience worthy of the new name of *computational neurobehaviour*.

In an attempt to build a model combining brain, realistic biomechanics *and* sensory feedback, we sought to extend our previous work modelling the oculomotor system by adding a virtual, biomechanical eye model able to make physically realistic movements. The rotational state of the eye would then determine how visual features in the virtual world were projected back into the brain model. The existing model (Cope et al., 2017) is already able to capture sensory input and convert it into a neural signal, assumed to specify the target of a *saccadic eye movement*; a fast movement of the eyes which directs the fovea to a region of interest in the field of view. The oculomotor system is an excellent candidate for modelling

64 because its movements can be specified with only three degrees of freedom, making it one of the simplest
65 neuro-muscular systems in the body. It is nevertheless behaviourally interesting, as saccadic eye movements
66 reveal information about decision making at a subconscious level (Deubel and Schneider, 1996; Reppert
67 et al., 2015; Marcos and Genovesio, 2016). The modelling of the oculomotor system is served by a large
68 body of behavioural data describing saccades (Tipper et al., 2001; Walker et al., 1997; Casteau and Vitu,
69 2012), many anatomical studies of the neural substrates involved (Meredith and Ramoa, 1998; Isa, 2002;
70 Isa and Hall, 2009) and electrophysiological data linking these together (Hepp and Henn, 1983; Dorris et al.,
71 1997; McPeek et al., 2003; Vokoun et al., 2011). Furthermore, in the context of building *behaving* systems,
72 a realistic mechanism for gathering visual information is a necessary part of any model for which the
73 behaviour requires visual attention and decision making. This is obvious from extrinsic considerations—a
74 subject must look at a scene to make decisions or navigate within it. It also follows for *intrinsic* reasons.
75 For example, Howard and Tipper (1997) showed that visual cues affect reach trajectories and the same
76 group later demonstrated that reaching affects the saccadic system (Tipper et al., 2001) suggesting a close
77 relationship between these neural systems. Building a behaving oculomotor system will therefore assist
78 future computational neurobehavioural modelling efforts that involve reaching.

79 Many neural populations are involved in the coding of saccadic eye movements, only a very brief
80 overview is given here; for a review, see Munoz (2002). One pathway takes information from the retina
81 directly into the superficial layers of the superior colliculus in the brainstem (Sterling, 1971; Linden and
82 Perry, 1983; Wu et al., 1994). Activity within the superior colliculus then excites neurons in the pons,
83 medulla and rostral mid-brain (Sparks, 2002) and finally the motor neurons, which innervate the extraocular
84 muscles (Fuchs and Luschei, 1970; Sparks, 2002). This direct pathway is responsible for the low latency
85 saccades called express saccades (Schiller et al., 1987; Edelman and Keller, 1996). Information from the
86 retina is also processed by visual cortex which feeds through to the frontal eye fields in which activity is
87 related to reflexive and voluntary saccades (Schall and Thompson, 1999). Activity build-up in the frontal
88 eye fields is transferred to the intermediate layers of the superior colliculus (Stanton et al., 1988b) and is
89 also processed by the basal ganglia, which participates in the selection of the winning saccade end point
90 (Stanton et al., 1988a; Hikosaka et al., 2000). Although both cortical and subcortical paths produce a
91 saccade target signal in the superior colliculus, it is also possible for animals to make relatively normal
92 saccades even after the colliculus has been ablated (Wurtz and Goldberg, 1972; Aizawa and Wurtz, 1998),
93 though express saccades are lost with collicular lesions (Schiller et al., 1987). This makes the superior
94 colliculus a perplexing structure, being both critically involved in saccade target specification (Sparks and
95 Nelson, 1987) and saccade dynamic control (Waitzman et al., 1991; Goossens and van Opstal, 2012) and
96 yet dispensable. The ‘backup pathway’ likely incorporates the oculomotor vermis and fastigial oculomotor
97 region of the cerebellum which are known to participate in the specification, dynamics and adaptation of
98 saccadic eye movements (Kleine, 2003; Takagi et al., 1998).

99 There is a long history of modelling the oculomotor system. For a comprehensive review, see Girard and
100 Berthoz (2005). Models of individual sub-systems have been proposed for brainstem (Robinson, 1975;
101 Scudder, 1988; Gancarz and Grossberg, 1998), cerebellum (Quaia et al., 1999; Dean, 1995; Dean et al.,
102 1994) and superior colliculus (Massone, 1994; Arai et al., 1994; Morén et al., 2013; Marino et al., 2012).
103 More recently, combined models have also been developed incorporating sensory input (Cope et al., 2017)
104 and driving a second order differential equation representing the eye (Tabareau et al., 2007; N’Guyen
105 et al., 2014; Thurat et al., 2015). None of these models has yet fully closed the loop to produce a behaving
106 system operating freely within its environment. We argue that developing integrated, closed-loop models of
107 behaving systems offers insights into the operation of neural systems that are not available from input- or
108 output-assumption models.

2 MATERIAL & METHODS

The integrated brain and biomechanical model described here is a development of the model in Cope et al. (2017), referred to here as the *Cope-Chambers model*. This was a rate-coded neural network model incorporating retinal populations, frontal eye fields (FEF), the basal ganglia (BG), and the superior colliculus (SC). The Cope-Chambers model takes as *input* the positions of luminances (of fixed shape and intensity) on a topographic map. While certain assumptions were made about the input—that a luminant input excites activity on a retinotopic layer, with computer code carrying out the transformation achieved in the brain by a neural connectivity map (Thivierge and Marcus, 2007)—it is nonetheless *not* an input-assumption model according to our definition because the activity generated in the neural input layer is modelled as a response to the luminances, rather than being crafted. In the Cope-Chambers model, the centroid of the activity in the deep layers of superior colliculus was assumed to accurately encode the location of the eye at the end of the saccade (Wurtz and Goldberg, 1972; Robinson, 1972; Van Gisbergen et al., 1987; McIlwain, 1982). This location was used to recalculate the positions of the luminances in the eye’s frame of reference at each time step. Because a pattern of neural activity in the output population was assumed to have a behavioural outcome, it was thus an *output-assumption model*. The model included no brainstem populations other than superior colliculus, nor a neuromuscular model.

To the Cope-Chambers model, we added a brainstem model and a biomechanical eye model. The rate-coded brainstem model was taken from the literature (Gancarz and Grossberg, 1998) as the best-of-breed saccadic burst generator (Girard and Berthoz, 2005). The biomechanical eye was implemented using the biomechanical modelling framework OpenSim; the brain and brainstem were modelled using the SpineML toolchain. These will be described below, along with a review of the Cope-Chambers model, but first we will give a description of the co-ordinate systems that were used.

2.1 Co-ordinates in the world

Before describing the biomechanical eye and the brain model, which consisted of retinotopically mapped neural sheets, we describe the co-ordinate system used in the world. The eye was located at the origin of a three-dimensional, right-handed Cartesian co-ordinate system, with its fovea directed in the $-z$ direction. There was a notional spherical screen which was also centred at the origin of the co-ordinate system and had a radius of 50 (in arbitrary units). The *fixation point* was the point on the screen at which the eye was initially directed. Onto the screen were projected target luminances, each of which having a position described by two co-ordinates; θ_x^t , a rotation of the horizon plane about the x axis, and θ_y^t , a rotation of the meridian plane about the y axis. The position is the intersection of these rotated planes with the spherical screen (disregarding the intersection point of these three surfaces behind the eye). Note that a luminance with positive θ_x^t was above the horizon of this world; one whose θ_y^t was positive lay to the left of the world’s meridian. For this reason, many of the figures in this paper are plotted with $-\theta_y$ on the x -axis and θ_x on the y -axis so that targets that lay up and to the right in the world do so in the graphs, also.

Luminances were crosses of height and width subtending $\pm 3^\circ$ and whose ‘bars’ were 2° thick. Luminances were oriented like + symbols with their vertical bar aligned with the meridian plane and their horizontal bar aligned with the horizon.

The eye’s frame of reference was initially aligned with the world’s frame of reference. At each timestep, the eye’s rotational state (described by the Euler rotations θ_x , θ_y , θ_z) was used to translate the three dimensional Cartesian co-ordinates of the luminances in the world frame into co-ordinates in the eye frame.

149 The luminance co-ordinates in the eye's frame of reference were used to determine the input to the brain
150 model.

151 2.2 Existing brain model

152 The brain model, excluding the brainstem, is a re-implementation of the Cope-Chambers model of
153 reflexive saccadic behaviour (Cope et al., 2017). Reflexive saccades are fast eye movements elicited by
154 abrupt changes in the peripheral visual scene (reflexive saccades can occur also as a result of auditory
155 and somatosensory stimuli, but these modalities are ignored in this model). A reflexive saccade has a
156 starting position defined by the initial orientation of the eye and an end-point position in which the eye
157 is directed towards a new target. Regardless of the number of targets within the visual scene, the brain
158 must choose one location as the end-point, because the eyes can look only in one direction at a time. The
159 functionality reproduced by the Cope-Chambers model is 'the selection of the best target end-point for
160 a reflexive saccade'. A competition such as this between incompatible movements is often referred to
161 as an *action selection* problem (Norman and Shallice, 1986; Maes, 1989; Redgrave et al., 1999). The
162 Cope-Chambers model is therefore a model of action-selection in the oculomotor system for reflexive
163 saccades. One hypothesis for the rôle played by the basal ganglia (BG) is that the system performs *action*
164 *selection* (Mink, 1996; Redgrave et al., 1999; Hikosaka et al., 2000). The Cope-Chambers model places the
165 BG at the centre of the oculomotor system; this follows the known anatomy of the region (Hikosaka et al.,
166 2000) and provides a mechanism for action selection of the best saccade. The BG receives input indirectly
167 from the superior colliculus, which has a retinotopic arrangement (Ottes et al., 1986).

168 The BG receives excitatory inputs directly from retinotopic regions of the cortex including the frontal eye
169 fields (FEF), supplementary eye fields (SEF), lateral intraparietal cortex (LIP) and dorsolateral prefrontal
170 cortex. The dorsolateral prefrontal cortex, which participates in voluntary saccades (Funahashi et al., 1993;
171 Munoz and Everling, 2004), is not modelled because the model concerns reflexive rather than voluntary
172 eye movements. Several other regions of the brain that are associated with eye movements are also omitted
173 from the model. The early visual processing stream in cortex, from V1, through to the LIP is subsumed into
174 a 'sustained retinal' signal which arrives at FEF. The justification here is that the model reacts to simple
175 luminant targets and does not need to carry out the feature extraction performed by these visual areas. The
176 supplementary eye fields are involved in the programming of saccade sequences (Tehovnik et al., 2000)
177 and memory guided saccades (Chen and Wise, 1995; Schlag, 2002). Lesions of SEF do not affect visually
178 guided saccades (Gaymard et al., 1998) and so the SEF is also omitted from the model.

179 Fig. 1(a) shows the macroscopic architecture of the Cope-Chambers model. The figure shows the
180 relationships between the retinal input populations, the FEF, the populations comprising the BG sub-system
181 (the red border indicates that the box represents a number of populations as a sub-system), the thalamus and
182 the superior colliculus. Excitatory connections are indicated with arrowheads; inhibitory connections with
183 circles in place of the arrowheads. The blue and green connection lines indicate two thalamo-basal ganglia
184 loops, one cortical loop through FEF (green), the other a sub-cortical loop through SC. It is important to
185 note that although they are given different colours in the diagram, these loops are in no way independent,
186 with loop activity combining both in thalamus and in the basal ganglia and a direct excitatory, feed-forward
187 connection from FEF to SC.

188 The basal ganglia sub-system is the most complex component of the Cope-Chambers model. The BG
189 model is based on previous work (Gurney et al., 2001b,a) and is referred to as the GPR model. The GPR
190 model incorporates the following main components of the primate BG (Mink, 1996; Wickens, 1997): (i)
191 The striatum (the main input station to the BG) which is divided into two iterdigitated populations of

192 projection neurons expressing primarily D1 or D2-type dopaminergic receptors (named Str_D1 and Str_D2);
193 (ii) The subthalamic nucleus (STN); (iii) the external segment of the globus pallidus (GPe); (iv) the output
194 nucleus relevant for saccadic control—the substantia nigra pars reticulata (SNr) (Hikosaka et al., 2000).

195 The connectivity of the GPR model [Fig. 1(b)] is constrained by the known anatomy and physiology of
196 the BG (Bolam et al., 2000). Physiologically, the only source of glutamate within the BG is the STN, whose
197 projections are therefore excitatory; all other nuclei have GABAergic projection neurons and are therefore
198 inhibitory. The cortex sends glutamatergic projections to both the Str_D1 striatal population, which projects
199 preferentially to the SNr, and to Str_D2, which projects primarily to GPe (Gerfen et al., 1990). The cortex
200 also projects to the STN, which sends diffuse projections to the SNr and GPe (Parent and Hazrati, 1993).
201 The GPe projects to the SNr and also projects back to the STN, completing a GPe–STN loop.

202 The GPR model is arranged into ‘action channels’; Fig. 1(b) shows an example network containing three
203 channels. It is between these channels that competition occurs, with the winning channel succeeding in
204 reducing activity in the output nucleus, SNr, and thereby disinhibiting its target. The complete connectivity
205 pattern for this small network is shown in Fig. 1(b); the left channel in cortex innervates the left channels
206 of Str_D1, STN and Str_D2. Connections are one-to-one, so it follows that the middle channel of cortex
207 innervates the middle channels of STN and the striatal populations and the right channel of cortex innervates
208 right channels in striatum and STN. Striatal population channels also inhibit SNr and GPe on a one-to-one
209 basis and GPe feeds inhibition to SNr and STN in a one-to-one manner. The outputs from STN however
210 are not one-to-one. The output from all channels of STN is summed together and then the sum is fed into
211 each channel of SNr and GPe. This models the diffuse excitation from STN which has been observed in
212 the BG (Parent and Hazrati, 1993).

213 Within the BG, there are several mechanisms supporting competitive processing for selecting channels
214 whose inhibitory output should be reduced. The selection mechanism of the GPR model is the ‘off-centre,
215 on-surround’ scheme proposed by Mink and Thach (1993). The ‘on-surround’ is provided by diffuse,
216 excitatory projections from the STN to the SNr. Focussed inhibition from the Str_D1 neurons in striatum
217 contributes the ‘off-centre’ part of the mechanism. This arrangement leads to selection behaviour via a
218 release of target inhibition, since channels that have strong salience (input) have weak output at the level of
219 SNr, and channels with weak salience have enhanced output.

220 The GPe is not included in the centre-surround circuit described above, but still plays a key rôle in
221 selection. Operating alone, the Str_D1/STN/SNr circuit can suffer from the following problem: if the input
222 for all channels is relatively high, then the diffuse projection from STN, which effectively supplies a sum
223 of *all* of the STN inputs to each channel in SNr, will provide so much excitation that Str_D1 may become
224 unable to inhibit one of the channels in SNr and selection may become impossible. Gurney et al. (2001b,a)
225 showed that the inhibitory feedback from GPe to STN acts as an ‘automatic gain control’ to help prevent
226 this from occurring.

227 At the neuronal level, the STN, GPe and SNr have tonic output activity (Chevalier and Deniau, 1990;
228 DeLong et al., 1985; Kita and Kitai, 1991). This is modelled using piecewise linear output functions
229 with zero offsets, c (see Eq. 6) but with noise added to the input. In striatum, Str_D1 and Str_D2 have
230 positive offset c , mimicking the so-called ‘down-state’ of medium spiny neurons which have a resting
231 potential far below spiking threshold and require co-ordinated input to generate action potentials (Wilson
232 and Kawaguchi, 1996). In addition, the Str_D1 and Str_D2 neurons are influenced by dopamine in different
233 ways; facilitating cortico-striatal transmission at medium spiny neurons with D1 receptors (Hernández-
234 López et al., 1997; Gonon, 1997) and reducing transmission at those with D2 receptors (Delgado et al.,

235 1999). These effects are modelled using a dopamine parameter, d , which modulates the input activations
 236 a_{in}^{D1} and a_{in}^{D2} as:

$$237 \quad a_{in}^{D1} = (0.2 + d)A \quad (1)$$

$$a_{in}^{D2} = (1 - d)A \quad (2)$$

238 where A is the input activation (see also Eqns. 10 & 11). For the ‘normal, healthy’ value for d of 0.7,
 239 Str_D1 activation is relatively enhanced ($0.9A$); Str_D2 activation is one third of this value ($0.3A$). The
 240 major effect of this difference in the relative strength of the activity in Str_D1 versus Str_D2 is simply that
 241 a change in the level of activity in Str_D1 affects the off-centre, on-surround mechanism. The effect of
 242 varying the input into Str_D2 is much more subtle, with only a small change in the amount of inhibition fed
 243 from GPe into STN (via a focussed, one-to-one connection) being affected by the change, along with a
 244 small change in the inhibition fed into SNr from GPe (also via a one-to-one connection). It is not possible
 245 to ascribe the dynamic effect of the dopamine parameter to any single population, because the activity is
 246 recurrently connected through multiple loops. Thus, a line of reasoning such as “reduced activity for a
 247 luminance in Str_D2 will lead to less inhibition in that region in GPe, which means that there will be higher
 248 activity there, and hence more inhibition for that region passed to STN leading us to expect less activity in
 249 STN” is verified by running a suitable simulation with the model, but the effect is small. Note that the
 250 effect of dopamine in the model is only to modulate the strength of cortico-striatal synapses; no learning is
 251 modelled and so the significance of dopamine as a prediction error signal is outside the scope of the current
 252 work.

253 The GPR model in Fig. 1(b) has only three channels, with the focussed inhibition from striatum to SNr
 254 and GPe defined by a simple one-to-one scheme. The action channels represent discrete, incompatible
 255 motor action choices. In the oculomotor model, an action channel represents the end-point of saccade,
 256 and the competition carried out in the basal ganglia is between potential saccade end-points. However,
 257 eye movements have a *continuous* end-point space; the eye can rotate to any orientation within its
 258 biomechanically permissible range. Some end-points within this range are mutually exclusive—it’s not
 259 possible to look to the left and to the right simultaneously—but *nearby* end-points are not necessarily
 260 incompatible. A small enough error in the end-point of a saccade will not prevent the eye from foveating on
 261 a target as the foveal region of high visual acuity is not infinitesimally small. To cope with this requirement,
 262 the populations within the oculomotor basal ganglia are conceived of as two-dimensional topographic
 263 grids of leaky integrator neural elements. Activity in each element corresponds to a spatial location in the
 264 visual field. Neighbouring elements correspond to locations which are close to each other in the visual field.
 265 Focussed one-to-one projections in the GPR model are replaced by projective fields with many weighted
 266 connections. Specifically, each unit in Str_D1 projects to a counterpart SNr_j in SNr with some weight
 267 w_{max} , but also connects to neighbouring nodes in SNr with a weight given by $w_{max} \cdot G(d)$, where $G(d)$
 268 is a circularly symmetric, 2D-Gaussian which is a function of distance d from SNr_j [Figs. 1(c)&(d)]. A
 269 similar scheme applies for the connectivity from Str_D2 to GPe and for a number of the other connections
 270 in the Cope-Chambers model; in the SpineML implementation of the model, this connectivity scheme is
 271 named ‘GaussianKernel’. Fig. 2 shows a schematic of the SpineML implementation of the model, based on
 272 a diagram produced by SpineCreator. Populations for Str_D1, Str_D2, STN, SNr and GPe are shown within
 273 the ‘Basal Ganglia’ box. Input comes into the model via the ‘World’ population and the output population
 274 is SC_deep. Compare this diagram with Figs. 1(a) & (b). Fig. 2 expands the ‘SC’, ‘BG’ and ‘slow retinal’
 275 boxes from Fig. 1(a).

276 The frontal eye fields (FEF) are a key cortical area for the generation of saccadic eye movements
 277 (Hikosaka et al., 2000; Tehovnik et al., 2000; Robinson and Fuchs, 1969; Bruce and Goldberg, 1985).

278 Saccadic targets are retinotopically mapped on its surface (Robinson and Fuchs, 1969; Bruce and Goldberg,
279 1985; Sabes et al., 2002), and increased neural activity at a location on the map precedes a saccade to that
280 location. Importantly, the FEF is also associated with visual decision making (Thompson and Bichot, 2005;
281 Schall et al., 1995; Monosov et al., 2008; Cohen et al., 2009). Thus, in a saccade choice, increased FEF
282 activity is predictive of the eye movement whether correct or incorrect (Thompson et al., 2005), rather than
283 of the correct response.

284 FEF neurons can be divided into three functional groups, related to whether their activity corresponds
285 with visual stimuli, motor action, or both (Segraves and Goldberg, 1987). The Cope-Chambers model
286 simplifies this categorisation using a single layer of 50 by 50 units representing the mean of all three
287 groups. This layer therefore responds to both visual stimuli and the buildup of activity associated with
288 motor (saccadic) action. The retina provides a persistent luminance signal into the FEF through the dorsal
289 visual pathway (Ungerleider and Mishkin, 1982) which is abbreviated in this model to a direct connection
290 with delay and noise.

291 The FEF provides input into the BG (Saint-Cyr et al., 1990) (to Str_D1, Str_D2 and STN) which, in turn,
292 projects back to thalamus in a retinotopically organised way (Middleton and Strick, 2000; Lynch et al.,
293 1994). In addition, the thalamic targets of this path are regions with strong reciprocal connections to the
294 FEF (McFarland and Haber, 2002). In this way, the FEF forms channel-based loops through basal ganglia
295 of the kind described above. Such circuits formed the basis of the model of Humphries and Gurney (2002).
296 The thalamo-cortical loop may be thought of as an integrator of information, whose gain is modulated by
297 inhibition from basal ganglia (Chambers et al., 2012; Cope and Gurney, 2011).

298 The superior colliculus (SC) is a sub-cortical nucleus which also plays a critical rôle in the generation
299 of saccades (Hikosaka and Wurtz, 1983). Both FEF and SC have direct connections to the saccadic burst
300 generator (SBG, see Sect. 2.3). If either is lesioned, the other can direct gaze, following a period of
301 adjustment (Latto, 1977), albeit with some persistent deficits. The SC is also a direct target of output
302 from the SNr (Jayaraman et al., 1977; Jiang et al., 2003) and can be influenced by the action selection
303 mechanisms of the BG. In particular, it forms a loop with BG, but unlike its cortical counterpart in FEF, the
304 input to basal ganglia comes via the thalamus [Fig 1(a), blue arrows].

305 While the SC has seven alternating cell- and fibre-rich layers (Wurtz and Albano, 1980), in most cases
306 these are categorised as the ‘superficial’ and ‘deep’ layers, which have significantly different response
307 properties. Cells in the superficial layers, which receive input from the retina, are mainly visually responsive,
308 with a preferred response to phasic events (luminance onsets and offsets) and movement on the visual
309 field (Goldberg and Wurtz, 1972). In contrast, cells in the deep layers receive multi-modal input, including
310 inhibitory input from the output structures of the BG (Jayaraman et al., 1977), and are directly involved
311 in the generation of saccadic eye movements. Saccade related activity in the deep layers appears to
312 generate saccades through ‘population coding’, with a weighted sum of activity across the retinotopy of SC
313 determining the saccade target (Lee et al., 1988; van Opstal and van Gisbergen, 1990; Mays and Sparks,
314 1980). The deep layers of SC receive input from the FEF in a topographic manner (Stanton et al., 1988a;
315 Sommer and Wurtz, 2000).

316 The SC in the Cope-Chambers model is based on the the model described in Arai and Keller (2005), with
317 the difference that the SNr input to the SC is generated by the BG model, rather than being hand-crafted.
318 The SC model has a superficial and a deep layer, each of which is a 2-D array of 50 by 50 leaky integrator
319 units arranged in the same retinotopic manner as the FEF (Wurtz and Albano, 1980).

320 The Cope-Chambers model incorporates a special connectivity pattern for visual input to the BG via
321 cortical (FEF) and sub-cortical (thalamus) pathways. Due to the retinotopic mapping (Sect. 2.2.2), foveal
322 luminances deliver a strong signal to the BG; roughly one third of the map is activated for the foveal targets
323 used in this work (Fig. 3, red cross). This makes it virtually impossible for a peripheral target (Fig. 3,
324 yellow cross) to win selection in the BG. Even if the peripheral target competed successfully to generate a
325 saccade, this process would cause a significant delay, leading to latencies much larger than those observed
326 experimentally. To overcome this problem, the Cope-Chambers model incorporates a mechanism in which
327 the synaptic strength of connections between FEF, thalamus and striatum are reduced close to the fovea
328 according to a shifted hyperbolic tangent. This connection is named ‘DecayingAtFovea’ in the SpineML
329 implementation and follows a modified sigmoidal curve rather than tanh. In either case, the relation is
330 ‘S-shaped’ and normalised to the range [0 1]. Far from the fovea (where the S-shaped curve has the value
331 ≈ 1), the connectivity pattern looks almost identical to a one-to-one connection.

332 Input to the Cope-Chambers model is provided through a simple retina model which directly samples
333 from a larger ‘world array’ of pixel values. In the current model, the input for the retina is named ‘World’
334 and is the retinotopic projection [Fig. 2(b)] of the eye’s field of view of the world [Fig. 2(a)] and the
335 luminant targets therein. The raw input in ‘World’ is fed into a population which adds noise, and then
336 via a delayed connection to FEF (the sustained retinal input path), to simulate processing through the
337 dorsal visual stream. It is also fed, without substantial delay, into two leaky integrator layers (Retina_1
338 and Retina_2) with different time constants, with the more slowly reacting layer (Retina_2) inhibiting its
339 faster counterpart. The faster layer responds quickly to the appearance of a prolonged stimulus before it
340 is inhibited by the slow layer, forming a phasic response to stimulus onset. The mechanism ensures that
341 phasic rather than tonic responses arrive at the superficial SC from the retina.

342 The output of the Cope-Chambers model is determined by the activity in the SC_deep population. The
343 activity in SC_deep is first transformed from retinotopic co-ordinates into Cartesian co-ordinates. The
344 centroid of the activity is then computed. The position of this centroid in the Cartesian frame determines
345 the saccadic end-point. The current model differs in that it does not compute a centroid, instead feeding the
346 SC_deep activity into the saccadic burst generator.

347 The Cope-Chambers model was parameterised by tuning the model to perform a prosaccade task in
348 which a central luminance point was fixated by the model. After a fixed duration, the fixation point was
349 extinguished and a target point of fixed luminance was presented. The model was tuned so that the latency
350 between the presentation of the target and the initiation of an eye movement matched experimental data
351 (Reulen, 1984), while also matching the electrophysiological evidence of activity in a variety of brain
352 regions. The tuning of the BG model attempted to preserve as closely as possible the weights used in the
353 original paper (Gurney et al., 2001b). Further details on the parameterisation of the Cope-Chambers model
354 are given in Cope et al. (2017).

355 2.2.1 Components

356 With the exceptions of the World and FEF_add_noise populations, each neural element represents an
357 activation; the activation is governed by a first order differential equation specified in a *SpineML component*.
358 SpineML, which will be outlined in Sect. 2.5, provides a means to mathematically define the five distinct
359 components in use in the brain model.

360 The *LINlinear* component, which is used in FEF, Thalamus, SC, SNr and GPe populations, governs the
 361 activation a with a first order leaky integrator differential equation:

$$\dot{a} = \frac{1}{\tau}(a_{in} - a) \quad (3)$$

362 where τ is the time constant for the neural activation and a_{in} is the input to the neural element. a_{in} is
 363 defined by an activation input and a shunting inhibition input according to:

$$a_{in} = A(1 - s_a) + \alpha R_N \quad (4)$$

364 Here, A is the activation input and s_a is the shunting inhibition state variable whose value is related to the
 365 shunting input, S by

$$s_a = \begin{cases} S & S \leq 1 \\ 1 & S > 1 \end{cases} \quad (5)$$

366 R_N is a random number drawn from a standard normal distribution ($\sigma = 1$, $\mu = 0$) and introduces noise to
 367 the activation of the neural element, with the parameter α controlling the noise amplitude.

368 The output, y , of LINlinear is related to the activation a by the piecewise linear transfer function

$$y(a) = \begin{cases} 0 & a < c \\ a - c & c \leq a \leq 1 + c \\ 1 & a > 1 + c \end{cases} \quad (6)$$

369 where c is a parameter defining the offset of the transfer function. If $c < 0$, then for zero activation ($a = 0$),
 370 the output will be positive. This simulates the effect of a neural population having tonic firing. If $c > 0$
 371 then the output will be zero until the activation exceeds c , simulating neurons which only fire when driven
 372 by excitatory input.

373 The *LINret* component used for the retinal populations is similar to the LINlinear component, but with no
 374 intrinsic noise and no shunting inhibitory input. It has a neural input which is identical to the activation
 375 input A :

$$a_{in} = A \quad (7)$$

376 The *LINexp* component is a leaky integrator with an exponential transfer function. It shares the same
 377 differential equation with LINlinear, but has a different input equation and a different output transfer
 378 function. It has the following equation for the neural element input a_{in} :

$$a_{in} = [A + N(a - V_r^-)](1 - S) + 0.01R_N \quad (8)$$

379 where A is the activation input and N is an input which is modulated by V_r^- , a reversal potential, and
 380 a , the current activation of the element. These inputs are summed and then reduced by a factor which
 381 is dependent on S , the shunting input. As in LINlinear, R_N introduces normally distributed noise to the
 382 element.

383 The output, y , of the LINexp component is given by

$$y(a) = \begin{cases} e^a - 0.9 & e^a \leq 1 + 0.9 \\ 1 & e^a > 1 + 0.9 \end{cases} \quad (9)$$

384 This component is used in the subthalamic nucleus (STN) population, as it gives a more physiologically
 385 accurate f-I behaviour (Wilson, 2004; Bevan and Wilson, 1999; Hallworth et al., 2003) which has been
 386 shown to allow the mapping of the basal ganglia network architecture onto an optimal decision making
 387 model (Bogacz and Gurney, 2007).

388 The *DIMSN* and *D2MSN* components are both leaky integrators, similar to LINlinear. They differ in
 389 that they have no shunting inhibition. They are used to model medium spiny neuron (MSN) populations
 390 in the striatum. As they model the fact that most MSN neurons fall into two groups; those expressing D1
 391 dopamine receptors and those expressing D2 receptors, they have a dopamine parameter that modulates the
 392 input activation, so that their equations for a_{in} are thus:

$$a_{in}^{D1} = (0.2 + d)A + 0.01R_N \quad (10)$$

393

$$a_{in}^{D2} = (1 - d)A + 0.01R_N \quad (11)$$

394 where d is the dopamine parameter. Varying dopamine from 0 to 1 enhances the activation in the D1 model,
 395 whereas it decreases the activation of the D2 model elements, in line with experimental observations
 396 (Harsing and Zigmond, 1997; Gonon, 1997). Note that the equation for a_{in}^{D1} differs from that used in the
 397 Cope-Chambers model, for which the cortico-striatal weights are multiplied by $(1 + d)$ rather than $(0.2 + d)$.
 398 A typical value of d is 0.7.

399 In the typical components given above, the value of the activation A (and where relevant, the shunting
 400 input, S) is determined by summing the weighted inputs to the population:

$$A = \sum_i w_i^{act} x_i^{act} \quad (12)$$

401

$$S = \sum_i w_i^{sh} x_i^{sh} \quad (13)$$

402 w_i^{act} and w_i^{sh} are, respectively, the weights of the i^{th} activation or shunting connections received by the
 403 component; x_i^{act} and x_i^{sh} are the signals input to the activation and shunting connections.

404 2.2.2 Population activity and retinotopic mapping

405 Each population of 2500 neural elements was arranged in a 50 by 50 grid, with positions on the grid
 406 representing a retinotopic mapping similar to that found empirically both in the superior colliculus (Ottos
 407 et al., 1986) and in visual cortex (Schwartz, 1980) and assumed in this work to persist throughout the
 408 oculomotor system.

409 In a retinotopic mapping, the Cartesian co-ordinates of the light-sensitive cells in the retina, whose density
 410 varies with distance from the fovea, are transformed into the Cartesian co-ordinates of the correspondingly
 411 active cells on the colliculus. The mapping ensures that an even density of cells can be maintained in the
 412 colliculus, but ensures that a group of adjoining, active, retinal neurons will always activate an adjoining
 413 group of neurons on the collicular surface.

414 The mapping turns out to resemble polar co-ordinates. That is, one axis of the collicular surface specifies
 415 the eccentricity of a retinal location (how far it is from the fovea) and the second axis specifies the rotational
 416 angle of the retinal location; we therefore use the convention of referring to the eccentricity axis on the
 417 colliculus as r and the rotation axis as ϕ .

418 The *cortical magnification factor*, $M(r)$, gives the relationship between the radial eccentricity r and the
 419 retinal neural density. As in Cope et al. (2017), we use a first-order approximation of the form for $M(r)$
 420 given in Rovamo and Virsu (1979):

$$M(r) = \frac{M_f}{1 + \frac{r}{E_2}} \quad (14)$$

421 The foveal magnification, M_f , is the magnification of the most central region of the retina and has a value
 422 in the human of about 7.8 mm° (Rovamo and Virsu, 1979).

423 In our model, M_f is related to W_{nfs} , the width of the retinotopic neural field, W_{fov} , the width of the
 424 eye's field of view and E_2 , the eccentricity at which the retinal density has halved by:

$$M_f = \frac{W_{nfs}}{E_2 \ln \left(\frac{W_{fov}}{2E_2} + 1 \right)} \quad (15)$$

425 Here, W_{nfs} is 50 (the side length of the 50x50 grid) and W_{fov} is set to 61° , a reduction from the biologically
 426 accurate 150° due to the small number of neurons in the retinotopic neural field. E_2 is 2.5 (Cope et al.,
 427 2017; Slotnick et al., 2001).

428 The mapping from the retinotopic co-ordinates in the brain to rotational co-ordinates of the stimu-
 429 lus/response was written down by Schwartz (1977, 1980) for measurements of striate cortex [visual
 430 stimulus to electrophysiological response—Daniel and Whitteridge (1961); Talbot and Marshall (1941)]
 431 and by Ottes et al. (1986) for superior colliculus data [electrophysiological SC stimulus to eye movement
 432 response—Robinson (1972)]. We used the following statement of this mapping to introduce stimuli into
 433 the ‘World’ input population of the brain model:

$$\phi = \frac{W_{nfs}}{2\pi} \arctan \left(\frac{\theta_y^t}{\theta_x^t} \right) \quad (16)$$

434

$$r = M_f E_2 \ln \left(\frac{1}{E_2} \sqrt{\theta_x^t{}^2 + \theta_y^t{}^2} + 1 \right) \quad (17)$$

435 Note that we use r and ϕ as the co-ordinates on the ‘collicular surface’. Schwartz uses r and ϕ as the polar
 436 co-ordinates of the retinal stimulus; Ottes et al. use r and ϕ as polar co-ordinates for the eye movement
 437 response; both use u and v as the Cartesian co-ordinates of the neural map. We use θ_x^t and θ_y^t to give Euler
 438 rotations for the retinal target stimulus. Note also that the form of Eqns. 16 & 17 is slightly different from
 439 that given in Ottes et al. (1986) because our θ_x^t and θ_y^t are not the polar co-ordinates used in that work.

440 The mapping encompasses the entire visual field; the value of ϕ is allowed to vary from 0° to 360° along
 441 its axis. Effectively, the two contralateral colliculi found in the biology are incorporated into a single,
 442 square map, avoiding the need to carry out the kind of ‘colliculus gluing’ described in Tabareau et al.
 443 (2007).

444 It is straightforward to show that the reverse mapping is given by:

$$\theta_x = E_2 \left(e^{\frac{r}{M_f E_2}} - 1 \right) \cdot \cos \left(\frac{2\pi\phi}{W_{nfs}} \right) \quad (18)$$

445

$$\theta_y = E_2 \left(e^{\frac{r}{M_f E_2}} - 1 \right) \cdot \sin \left(\frac{2\pi\phi}{W_{nfs}} \right) \quad (19)$$

446 where we have dropped the t superscript on θ_x & θ_y , as these equations transform a collicular location into
447 rotations of the eye.

448 Fig. 3 shows the result of the mapping for a view of two cross-shaped luminances. One cross illuminates
449 the fovea, which results in a large comb-shape of activity. The more peripheral cross produces (in FEF) an
450 indistinct object centred at a larger value of r .

451 2.2.3 Network

452 Briefly, the model consists of input from the World population (see Fig. 2, green population box)
453 producing activity in an ‘express’ pathway to superior colliculus (purple) and simultaneously in cortex,
454 represented here by the FEF population (grey boxes in Fig. 2). The express pathway causes short latency
455 activity in the superficial superior colliculus, which directly innervates the deeper layers of the superior
456 colliculus (SC_deep). Activity in FEF generates firing in a thalamo-cortico-basal ganglia loop. The output
457 of the basal ganglia is the substantia nigra pars reticulata (SNr) which tonically inhibits SC_deep. If a
458 location of activity in FEF is able to dominate selection in the basal ganglia circuit, the corresponding
459 location in SNr will dis-inhibit and activity will build up in SC_deep encoding the saccade end point.

460 Connections shown in red are one-to-one connections; dark blue projections indicate a connectivity
461 pattern which ‘fans out’ with a 2-D Gaussian kernel [Fig. 1(c)]; lighter blue connections from the STN to
462 SNr and GPe are diffuse, all-to-all connections and projections coloured green are one-to-one connections
463 that decay towards the fovea so that foveal activity in FEF does not swamp the basal ganglia which
464 would prevent peripheral luminances from ever being selected. Note that SC_deep contains two recurrent
465 connections; one is excitatory, with a Gaussian kernel mapping and the other implements tecto-tectal
466 inhibition, which increases the inhibition between activity in opposite hemispheres of the field of view
467 (Gian G. Mascetti and Jorge R. Arriagada, 1981; Olivier et al., 2000) helping to resolve competition
468 between saccades to the left and right. The tecto-tectal inhibitory connection is *not* present in the Cope-
469 Chambers model. In all other respects the model is as described in Cope et al. (2017). We have not listed the
470 parameters of the network in tabular form here, instead, the reader is referred to the SpineML declarative
471 specification of the model from the link given in SUPPLEMENTAL DATA. The easiest way to access this
472 information is by using SpineCreator.

473 2.3 Brainstem model

474 We implemented a saccadic burst generator (SBG) based on the connectivity outlined in Gancarz and
475 Grossberg (1998). The SBG network for two of the model’s six channels is shown in Fig. 4. In the brainstem
476 model, we use the word ‘channel’ to mean a set of populations of neurons which are involved in actuating
477 a single extraocular muscle. SBG channels are arranged in pairs, actuating opposing muscles. There is
478 one pair of channels which actuates the superior and inferior rectus muscles, causing vertical rotations
479 of the eye in a roughly parasaggital plane (the eye moves up or down). Another pair actuates the lateral
480 and medial rectus muscles, causing horizontal rotations of the eye. The third pair actuates the superior

481 and inferior oblique muscles which contribute to vertical as well as oblique rotations. Activity from the
 482 output layer of superior colliculus (SC_avg) is fed into each channel, which sums the activity it receives and
 483 processes it in populations each of a single neural element representing all the neurons in that population.
 484 Each channel of the SBG functions to create the motor neuron activations that are required to accelerate
 485 the eye in a particular direction, then hold the eye in its new position against the returning force generated
 486 by the elastic properties of the muscles. The required motor neuron activations are therefore a combination
 487 of features: a brief burst of increased activity that accelerates the eye; followed by a period of activity that
 488 is less than the burst firing rate but higher than the tonic rate that exists when the eye is at the centre. This
 489 holds the eye in its new position.

490 The SBG connectivity produces each of the these features separately, then sums them to create the desired
 491 ‘bump and tonic’ activation time series. The input to the first population in the SBG, the long-lead burst
 492 neurons (LLBNs), is conceived as originating from one of the deep layers of the superior colliculus. The
 493 activity of the LLBNs are passed to excitatory burst neurons (EBNs) which, in turn, inhibit the LLBNs via
 494 the activity of the inhibitory burst neurons (IBNs). This feedback loop has a transmission delay, which
 495 allows activity to build up in the EBNs before the inhibition is activated and the activity is then reduced
 496 again. This mechanism generates the ‘bump’.

497 The generation of the ‘tonic’ phase of the required time series is achieved simply by integrating the bump
 498 over time and multiplying by a some small gain factor. This is the function of the tonic neurons (TNs).
 499 The firing rate of the motor neuron defines the amount of force applied to the eye by that muscle. Thus,
 500 the integral of the ‘bump’ defines how far the eye moves in that channel’s direction. The gain and delay
 501 parameters in the LLBN-EBN-IBN-LLBN feedback loop therefore have to be tuned such that the endpoint
 502 of the saccade is reasonably accurate. Furthermore the restoring force generated by the elasticity of the
 503 muscles is dependent on the radial distance. The value of the new tonic firing rate, after the ‘bump’ is
 504 dependent on the end location of the eye. If the ratio between the EBN firing rate and the TN firing rate is
 505 not exactly correct, the eye will drift away from the saccade endpoint after the saccade has been completed.
 506 The EBN-TN connection strength is therefore tuned such that the TN firing rate yields a stable eye position
 507 across a range of eye eccentricities.

508 The omnipause neurons (OPNs) are tonically active and inhibit the EBNs. The activity of the OPNs is
 509 itself inhibited by activity in the LLBNs. The purpose of this arrangement is to ensure the eye does not
 510 move in response to neural noise.

511 Each mean activity of all the neurons in each SBG population (except the TNs) is defined by a single
 512 leaky integrator, first order differential equation.

$$\frac{da}{dt} = \frac{1}{\tau}(y - a) \quad (20)$$

513 where a is the activation of the nucleus, and τ is the time constant of the nucleus. y is a piecewise linear
 514 function of the weighted sum of inputs to the nucleus and is given by

$$y(IN) = \begin{cases} 0 & IN \leq b \\ IN - b & b \leq IN \leq 1 + b \\ 1 & IN \geq 1 + b \end{cases} \quad (21)$$

515 where b is the IN axis offset. IN is the weighted sum of inputs to the nucleus and is given by,

$$IN = \sum_m^M w_{mn} a_m \quad (22)$$

516 where a_m is the activation of the m^{th} afferent nucleus. w_{mn} is the connection strength between the m^{th}
517 afferent nucleus and the current nucleus. The activity of the TNs are defined as

$$\frac{da}{dt} = \frac{1}{\tau} y \quad (23)$$

518 with the same piecewise linear transfer function as in the other SBG populations.

519 2.4 Biomechanical eye

520 The output signals of the brainstem's motoneuron (MN) populations are used to drive the biomechanical
521 model. The MN output signal in each brainstem channel is normalised in the range [0 1] and represents the
522 mean firing rate of the neurons that innervate the extraocular muscle for that channel. The biomechanics
523 are used not only to get tangible feedback on the simulated saccades including motion trajectories, but
524 to add one more modelling dimension related to the inertial properties of the eye plant including muscle
525 properties.

526 The biomechanical eye model, implemented using the OpenSim framework (Seth et al., 2011), is
527 anatomically represented by a sphere of uniform mass distribution. The diameter of the eye is 24 mm for
528 adults, with small variations between individuals; the mass of the eye is 7.5 grams. The eyeball is actuated
529 by six extraocular muscles (EOMs). The EOMs are arranged in three pairs forming a cone inside the orbit
530 with the apex being located inside the cranium in a tendonous ring called the annulus of Zinn. An important
531 feature of the oculomotor system which greatly affects its overall behavior is the existence of dynamic
532 EOM pulleys. Their role is to guide the pivot point of the EOMs. In our model, a pulley for each EOM has
533 been modeled by a point on the orbit whose location depends on the current eye orientation.

534 An illustration of the biomechanical eye model is given in Figure 5(a), while Figure 5(b) depicts the
535 head model used in the proposed framework. Figure 5(c) shows a cross-sectional view of the eye and the
536 spherical screen on which targets were projected.

537 Two types of muscle models of different complexity are supported. The first models muscles using linear
538 path actuators. This simplistic model of ideal muscles can be easily integrated with high level brain models.
539 As described above the muscles are wrapped around the eye. The more complex model supported is based
540 on the Thelen model (Thelen, 2003) that is also supported by OpenSim and implements Hill-type muscles.
541 It includes realistic muscle wrapping geometric entities of the muscle fibers, while it accommodates for
542 both activation and contraction dynamics. The dynamics of muscular forces can be split into: 1) The
543 elasticity of the muscles. 2) A delay between the onset of the afferent excitatory signal and the actual
544 muscle contraction, caused by the transmission time of the action potentials and by the necessary calcium
545 release at the muscle fibres.

546 The force applied by EOMs is controlled by an excitatory signal supplied by motoneurons in the brainstem.
547 The neural drive to produce a saccadic eye movement can be characterized by a pulse component to
548 overcome the viscoelasticity of the orbital plant, a step component to stabilize the eye in the new position,
549 and a slide component that models the gradual transition between the pulse and step.

550 Passive forces due to the fatty tissues inside the eye orbit also affect eye dynamics. Their role is critical in
551 eliminating the influence of head and body movements. We incorporated a custom torque, t , which acts
552 like a rotational spring-damper apparatus, resisting eyeball movements. It has elastic and viscous properties
553 governed by $t = -KR - CU$ where R is the eye's orientation and U is its angular velocity. K and C are
554 constants. A fuller description of the biomechanical model can be found in Papapavlou and Moustakas
555 (2014).

556 Finally, numerical integration of the biomechanical eye model is based on the Kutta-Merson integration
557 method.

558 2.5 Model development framework

559 The Cope-Chambers model was originally developed to run on the BRAHMS model execution framework
560 (Mitchinson et al., 2010; Mitchinson and James, 2015). To run a BRAHMS model, the researcher must
561 develop *BRAHMS components* for the various neural elements. A BRAHMS component is a program-
562 matically coded implementation of the behaviour of the component. It may have an arbitrary number
563 of inputs and outputs and may be written in C, C++, Python or MATLAB. The Cope-Chambers model
564 components were hand written in C++ and MATLAB. A BRAHMS *SystemML* file describes how the
565 different components connect together and how data is passed between them (Mitchinson et al., 2010). The
566 main BRAHMS program first reads the SystemML file, then dynamically loads all the required components
567 before executing the system.

568 In the current work, the Cope-Chambers model was reproduced using the declarative SpineML markup
569 language (Alex Cope and Paul Richmond, 2014; Richmond et al., 2014), with the help of the graphical
570 SpineML model editing software called SpineCreator (Cope et al., 2015, 2016a). SpineML, which is a
571 development of the NineML specification (INCF Task Force on Multi-Scale Modeling, 2011), describes
572 neural populations and their projections in a highly structured format in which neuron bodies, pre- and post-
573 synapses are described in terms of *SpineML components*. These are similar to the components provided by
574 BRAHMS, but in this case, the components are an XML description of the functionality of the component,
575 rather than a programmatic implementation, with one XML file per component. A SpineML *network layer*
576 file then describes which components are used in the model, and how they are connected together. Finally,
577 a number of SpineML *experiment layer* files specify how the model described in the network layer can be
578 executed. In the experiment layer, the execution duration and timestep can be specified, along with input
579 conditions, connection lesions and component parameter updates. A description of SpineML is given in
580 Richmond et al. (2014); the definitive definition is found in the schemas (Cope et al., 2014). SpineCreator,
581 in its rôle as a graphical editor for the SpineML format, was used to generate the SpineML files describing
582 the model. It was also used to generate the diagrams of the model.

583 As a declarative format for model specification, SpineML is agnostic about how the model is executed. A
584 number of simulation engines can be utilised, including DAMSON (Richmond, 2015), GeNN (Nowotny,
585 2011; Nowotny et al., 2014) and BRAHMS (used here). The simulation engine incorporating BRAHMS is
586 called SpineML_2_BRAHMS (Cope and James, 2015). SpineML_2_BRAHMS is a collection of XSLT
587 stylesheets which first generate and compile C++ BRAHMS components (which implement a simple,
588 Forward-Euler solver) from the SpineML component layer description files. SpineML_2_BRAHMS then
589 uses the SpineML network and experiment layer files to generate a BRAHMS SystemML description
590 of the model. Finally, SpineML_2_BRAHMS executes the model now described entirely as a BRAHMS
591 system, via a call to the BRAHMS binary. A number of additional, hand-written components are present in

592 SpineML_2_BRAHMS providing the inputs (constant inputs, time-varying inputs, etc) which the modeller
593 specifies in the experiment layer.

594 In addition to the brain model components, all of which are code-generated using SpineML_2_BRAHMS as
595 described above, two hand-written components are integrated into the model: The biomechanical eye model
596 and a sensory input component. The sensory input component takes the eye's rotational state and the state
597 of the experimental luminances and projects a retinotopic activity map into the brain model. Both of these
598 BRAHMS components were hand-written in C++. To incorporate these components into the SpineML
599 model, a SpineML_2_BRAHMS *external.xsl* file was used. The external.xsl file scheme for incorporating
600 external BRAHMS components into a SpineML model was a new SpineML_2_BRAHMS feature motivated
601 by the current work. Fig. 6 shows the workflow, in which the model specification files (blue box - a
602 combination of SpineML files and C++ code), are processed (green box) into a BRAHMS system (red
603 box).

604 2.6 Integrating the models and closing the loop

605 The Cope-Chambers model closes its loop by passing the centroid of activity in SC_deep (once it
606 has surpassed a threshold) back to the code that controls the world, which then uses this location to
607 instantaneously change the model's view of the world. In our extended model, it was necessary to connect
608 the output of the brain model back to its input via the saccadic burst generator model and the biomechanical
609 eye. The resulting state of the eye, rather than the centroid of the superior colliculus, was used to compute
610 the input to the brain, given the luminances visible in the world.

611 Thus, the information flow in the model is as follows: Luminances in the world have their locations
612 computed in the eye's frame of reference, based on the rotational state of the eye. The locations of the
613 luminances on the retina are transformed into a retinotopic co-ordinate system which determines the activity
614 in the 'World' population (named to mean the 'world as the brain sees it', rather than the world frame
615 of reference) which is the input for the brain model. The target luminance for a saccade is selected, as
616 described earlier, via cortical and sub-cortical loops through the basal ganglia model and activity for the
617 winning end-point builds up in the deep layer of superior colliculus. This activity excites the 6 channels
618 of the saccadic burst generator in the correct proportions for the saccade. The motoneurons, which are
619 the output of the SBG, send a rate-code signal (normalised between 0 and 1) into the biomechanical eye
620 model. The rotational state of the eye model is fed back to participate in the computation of the retinotopic
621 luminance activity in 'World', completing the loop.

622 A number of studies have considered the form of the connection between the deeper layers of the superior
623 colliculus and the saccadic burst generator (Van Gisbergen et al., 1985; Ottes et al., 1986; Waitzman et al.,
624 1991; Groh, 2001; Arai et al., 1994; Goossens, 2006; Tabareau et al., 2007; van Opstal and Goossens,
625 2008; Goossens and van Opstal, 2012), which has become known as the spatial temporal transform (STT).
626 The spatial aspect of the transform is thought to be implemented by a weight-mapping (Tabareau et al.,
627 2007; Arai et al., 1994). Although there is no definitive experimental proof for such a mapping, there
628 exists evidence for spatially variable synapse density (Moschovakis et al., 1998; Herrero et al., 1998) and
629 connection density (Grantyn et al., 2002) and we therefore adopt the idea. Arai and co-workers trained a 20
630 by 20 neural network model of the superior colliculus to discover the weight map under the assumption
631 of 2D Gaussian activation profiles (Arai et al., 1994)—that is, they assumed that the activity in superior
632 colliculus for any saccade was a size-invariant 2D Gaussian hill of activity. The training approach of
633 Arai et al. (1994) was not feasible in this study due to the length of time required to run our model and
634 its stochasticity, which meant multiple runs of the model were necessary in order to generate output

statistics. Tabareau et al. (2007) wrote down a theoretical form of the weight map, obtained by inverting the mapping of Ottes et al. (1986) and the assumption of invariant 2D Gaussian activity profiles in SC, which is equivalent to:

$$w(r, \phi) = i e^{jr} \sin(l\phi + k) \quad (24)$$

where r and ϕ are co-ordinates on the collicular map and i, j, k and l are parameters of the function (compare with Eq. 3 of Tabareau et al. (2007)). As they found it closely resembles the results of Arai et al. (1994), and it is a simple formulation, we considered it as the means to generate the six weight maps in our own model. One barrier to the use of this weight map was the Cope-Chambers model's violation of the *invariant integral hypothesis*. This states that the number of spikes emitted by a neural element during a saccade (or in our model, the integral of the neuron's output during the saccade) should be a function only of its position within the hill of collicular activity. That is, for any time-dependent hill of activity $\mathcal{A}(\mathbf{z}, t)$ at $\mathbf{z} = (r, \phi)$ on the collicular surface, the integrated activity $A_{\mathbf{x}}$ in an element at a vector \mathbf{x} away from \mathbf{z} is

$$A_{\mathbf{x}} = \int_t \mathcal{A}(\mathbf{z} - \mathbf{x}, t) dt \quad (25)$$

which is invariant for all \mathbf{z} . This requirement is fulfilled by spatially invariant 2D Gaussian profiles, whose time-course (how quickly they grow and then diminish) is always the same.

However, the very mapping on which the Tabareau et al. (2007) result is based leads to a very *variant* activity profile in the SC_deep layer of the Cope-Chambers model. A luminance of a given size which excites activity near to the fovea causes activity in a large number of neurons in each retinotopic layer, whereas activity far from the fovea excites a much smaller region. This effect is clearly demonstrated in Fig. 3 for equal sized targets both on and distal from the fovea.

To understand the need for this invariance, consider the effect of a 2D Gaussian hill in SC_deep which elicits a successful horizontal saccade of 10° using the weight maps shown in Figures 7(a)–(c). Activity from the 2D Gaussian (schematically represented as the large purple dashed circle in Figure 7C), passing through the weight maps will excite the superior (not shown) and inferior rectus [Figure 7(b)] channels by an equal, balanced amount, so these cancel out, allowing the eye movement to be horizontal. The amount of activation passed to the lateral rectus muscle results from a convolution of the Gaussian and the exponential component of the weight map relationship in Eq. 24. If the Gaussian hill now appears further along the collicular surface, coding for a 20° saccade, *and also becomes smaller* (small purple dashed circle), we can still argue that the vertical component signals to superior/inferior rectus muscles will cancel out, and we could imagine that the exponential component of Eq. 24 is correctly parameterised to compensate for the smaller hill. Now consider a 2-D Gaussian hill which codes for a 10° saccade which is 'down, and to the left' in equal proportions (large red circle). That means that the hill will sit on the boundary between the weight maps for the 'down', and the 'left' muscles. Now, if the hill moves to the $r = 20^\circ$ location on the colliculus (small red circle), *and also reduces in size*, it will excite only the periphery of the sine; the exponential increase of the map along r is not guaranteed to compensate for the reduction in the convolution of the Gaussian hill and the sinusoidally varying component of the weight map along the ϕ axis in Figure 7(a).

This led us to hypothesise that the retinotopic mapping to the SBG be preceded by an associated widening projection field such that the hill of activity in a 'final' deep layer of superior colliculus is invariant with position on the map. There are a number of locations in the system in which this widening projection field could exist. It could be implemented in the projections between the retinal populations and the

superficial layer of SC along with the projection between the World and the FEF population. However, this would affect activity within the basal ganglia of the model, contradicting a result in Cope et al. (2017) which explains the ‘hockey stick’ profile for saccade latency as a function of saccade eccentricity. Instead, we suggest that a widening projection field is encoded within the superior colliculus itself, a complex, multi-layered structure which could quite plausibly support such a function. Indeed, such widening activity can be seen in the stimulation experiments in Vokoun et al. (2010) and Vokoun et al. (2014). In Ghitani et al. (2014), from the same research group, evidence is presented for an excitatory and widely projecting pathway from the stratum griseum intermediale (equivalent to our SC_deep) to the more superficial layers stratum opticum and stratum griseum superficiale. Although this pathway is a ‘wide’ projecting field, the experiments do not indicate whether the projection *widens* along the rostral-caudal axis of the SC. Bayguinov et al. (2015) present evidence for another projecting field within SC whose connectivity pattern *does* change along the rostral-caudal axis. This projection is inhibitory in nature. Although neither of these results precisely match the widening, excitatory projection field hypothesised here, they do indicate that such connection patterns are plausible. Although in this work we do not model the SC in detail, we extended the model with a third functional layer named SC_deep2, shown in Fig. 7(b) (Cope-Chambers has only the two layers SC_sup and SC_deep). We introduced a widening projection based on a Gaussian projection field whose width, $\sigma(r)$ varies in inverse proportion to the magnification factor, $M(r)$, given in Eq. 14 according to:

$$\sigma(r) = \frac{m_\sigma}{M(r)} - \frac{m_\sigma}{M^0} + \sigma_0 \quad r > r_0 \quad (26)$$

m_σ is a scalar parameter which determines the ‘magnitude of the widening’. M^0 is the ‘starting’ magnification factor. Within the foveal region ($0 \leq r \leq r_0$), the projection field is not allowed to widen and so

$$\sigma(r) = \sigma_0 \quad r \leq r_0 \quad (27)$$

which makes σ_0 the width of the Gaussian projection field within the foveal region. (Note that the value chosen for the width of the foveal region, r_0 is not identical to the foveal shift parameter used in the *DecayingAtFovea* projections into striatum.) The *Widening Gaussian* projection weight, $w(r, d)$ is then computed as:

$$w(r, d) = e^{-\frac{d^2}{2\sigma(r)^2}} \quad (28)$$

where d is the distance between the source and destination elements in the collicular plane. m_σ was set to 50, σ_0 was 0.3, M^0 was 12.43 and r_0 was 20.

A further issue regarding the use of the theoretical weight map in Tabareau et al. (2007) was that it does not consider the existence of the oblique extraocular muscles. There is evidence that only two dimensional information is encoded in superior colliculus (Wurtz and Goldberg, 1972; Hepp et al., 1993; Van Opstal et al., 1991), but the eye is actuated by six extraocular muscles. In order to find out a possible form for the input to the oblique muscles we carried out a training process which depended on a centroid computation in SC_deep and was designed to maintain a null torsional eye rotation for all saccade end-points. For the four rectus muscles, the resulting weight map solutions resembled those found by Arai et al. (1994). The trained maps for the oblique muscles had a form very close to those for the inferior and superior rectus channels, but with a smaller magnitude. The inferior oblique map resembled the superior rectus map and the superior oblique map resembled the inferior rectus. When parameterising the theoretical weight maps, we set the inferior/superior oblique maps to be 1/10th of the superior/inferior rectus maps, respectively. Interestingly,

712 this suggests that there is a built-in synergy between the vertical and oblique channels in the eye, although
 713 the results will show there is some systematic change in the oblique error with saccade end-point location.

714 Tabareau et al. (2007) give a formulation for the weight maps in which it is possible to project both a
 715 positive and a negative weight. In our model, all projections from SC_deep are excitatory. This means that
 716 each channel has a weight which follows the form:

$$w(r, \phi) = i e^{jr} \sin\left(\frac{2\pi\phi}{W_{nfs}} + k\right) \quad (29)$$

717 where i , j and k are per-channel parameters for the weight maps. k is determined by the mapping. Only the
 718 positive part of the sine is utilised. i and j are parameters to be found.

719 The saccadic burst generator model was originally conceived with the assumption of a step input, which
 720 returns to zero activity at a suitable time to curtail the saccade and avoid staircase saccades (Gancarz and
 721 Grossberg, 1998). In our model there is no such mechanism to reduce activity in SC_deep, and elsewhere.
 722 Although a successful, accurate saccade towards a target luminance will remove the excitation which caused
 723 the activity in SC_deep by bringing the target luminance within the masked, foveal region, the activity
 724 in SC decays too slowly to avoid additional saccadic movements. We found it necessary to hypothesise
 725 an inhibitory feedback mechanism from the SBG to the brain model. This is shown in Fig. 4, which
 726 indicates how the output from the inhibitory burst neurons (IBN) of the SBG model are used to feed back
 727 an inhibitory signal to the SC_deep, thalamus and FEF populations in the brain model, resetting them ready
 728 for the next saccade. There is evidence for inhibitory projections to SC from the propositus hypoglossi
 729 nucleus (Corvisier and Hardy, 1991), which lies within the brainstem, upstream from motoneurons, and
 730 has been shown to encode eye velocity (Dale and Cullen, 2013).

731 The output signals from the six channels of the SBG were connected to the six motoneuron inputs of the
 732 biomechanical eye. The signal was normalised; a value of 1 meaning that all the motoneurons in the output
 733 population were firing at their maximum rate and the force exerted by the relevant extraocular muscle
 734 was maximal. Channels innervated extraocular muscles as follows: Up: superior rectus; Down: inferior
 735 rectus; Right: medial rectus; Left: lateral rectus; Z+: superior oblique; Z-: inferior oblique. Because the
 736 medial rectus induces a rightward rotation of the eye, our single virtual eye is a *left* eye. The OpenSim
 737 implementation of the biomechanical eye was ‘wrapped’ (in the software sense) in a BRAHMS component.
 738 This made it possible to integrate the OpenSim model into the BRAHMS framework. The wrapper ensured
 739 that the input and output signals were correctly transferred and, importantly, handled the disparity in the
 740 solver timesteps used in the OpenSim model (25 ms) and the neural model (1 ms). This was achieved by
 741 having the BRAHMS wrapper create a separate thread to run the OpenSim model. The BRAHMS wrapper
 742 component was called on each 1 ms timestep, receiving the instantaneous activations from the motoneurons
 743 in the SBG. These activations, and the current simulation time, were written into a shared memory area,
 744 accessible by the OpenSim thread. Running independently, the OpenSim thread would update its inputs
 745 (using the most recent values in the shared memory area) whenever the simulation time had increased
 746 by 25 ms. It would then recompute its outputs (the rotational state of the eye) and write these into the
 747 same shared memory. The BRAHMS wrapper would update its outputs whenever they were changed in
 748 the shared memory by the OpenSim thread. A direct connection of the six outputs of the BRAHMS eye
 749 model component to the six inputs of the worldDataMaker BRAHMS component was specified in the
 750 SpineML_2_BRAHMS external.xlsx file.

751 The eye model outputs its rotational state at each timestep. The rotational state is used to compute
752 the view of the world in the eye's frame of reference. To simplify the calculation, the luminances exist
753 on a spherical surface at the centre of which is the eye. A hand-coded BRAHMS component called
754 worldDataMaker computes the projection of the luminances into the eye's frame of reference and then
755 converts this representation into a retinotopic map to pass into the brain model. The input to the brain
756 model is thus able to change continuously, on every timestep, rather than in a step-wise fashion when a
757 saccade occurs, as in the Cope-Chambers model.

758 In the worldDataMaker BRAHMS component, the rotational state of the eye was used to construct
759 Euler rotation matrices which transformed between the world's frame of reference and the eye's frame of
760 reference. The worldDataMaker component received a specification of the world luminances in a JSON
761 file called luminances.json at the start of each simulation. This file specified the position, shape, size,
762 luminance, appearance time and disappearance time of an arbitrary number of luminances. With this
763 information, the instantaneous rotational state of the eye and the parameters of the retinotopic transform, it
764 was able to compute the instantaneous input to the brain model.

765 The final models, on which the results of this paper are based are named 'TModel3', 'TModel4' and
766 'TModel5'. Descriptions of these, and earlier versions of the model can be found in the code repository
767 given in SUPPLEMENTAL DATA.

3 RESULTS

768 3.1 Weight maps

769 We found the best parameters for the exponential in Eq. 29 (i and j) by a manual tuning process. After
770 selecting values for i and j in either the horizontal or vertical/oblique channels, we ran the model 6 times
771 at each of 8 target eccentricities (7° – 14°) which were purely in the direction of the newly parameterised
772 channel. The training saccades were produced as described below in Sect. 3.3, with the same fixation
773 and target luminances (crosses of magnitude 0.2 and 0.3) but with the fixation offset and target onset
774 occurring at 0.2 s. We measured the end-point of the saccade by detecting the location at which the saccade
775 velocity had dropped below 0.005 of its peak. We iterated until the mean saccade endpoint plotted versus
776 target was close to the ideal straight line—see Fig. 8(a) & (b). We applied the same parameters to both
777 directions of each channel; $i_{up} = i_{down} = 0.00195$, $j_{up} = j_{down} = 0.075$, $i_{left} = i_{right} = 0.0016$ and
778 $j_{left} = j_{right} = 0.067$.

779 The resulting weight maps (where the oblique maps are 1/10th of the vertical maps, as described earlier)
780 are shown in Fig. 9. First, recall that the r axis of the neural surface corresponds to the amplitude of a
781 saccade and the ϕ axis indicates the polar direction of the saccade, as described in Sect. 2.2.2 and Fig. 3.
782 Fig. 9(a) shows the weight map for the muscle which rotates the eye to the left. As we modelled a left
783 eye, this actuates the lateral rectus muscle. The exponential rise of Eq. 29 [for experimental evidence, see
784 Figs. 7 & 8 of Herrero et al. (1998)] is seen in the r direction; as r increases, so the connection strength to
785 the SBG channel rises exponentially. The connection strength is greatest along the centre line, for a value
786 of ϕ which corresponds to a purely leftward movement. Note that ϕ is presented in neural co-ordinates,
787 and not in degrees or radians; $1 \leq \phi \leq 50$ corresponds to a range of 0° to 360° ; $\phi = 38.5$ corresponds
788 to movements left. The connection strength drops away sinusoidally as ϕ moves away from the centre
789 line at $\phi = 38.5$. In regions of the map for which there is no leftward movement, that is, in the half of
790 the map which corresponds to any movement with a rightward component, the 'left' weight map is 0.
791 Fig. 9(d) shows the weight map for rightward movements, actuating the medial rectus muscle of the eye.

The line of maximum connection strength is along $\phi = 13.5$. The map is a mirror of Fig. 9(a), reflected about the line $\phi = 26$. The ‘left’ and ‘right’ weight maps are orthogonal; the non-zero region of the ‘left’ map is zero in the ‘right’ map and vice versa. Fig 9(b) & (d) show the weight maps for downward and upward eye movements; the ‘down’ map activates the SBG channel for the inferior rectus muscle, the ‘up’ map activates the superior rectus. Note that ‘down’ is not orthogonal either to ‘left’ or ‘right’ because a saccade down and left is achieved by simultaneously activating both the lateral and inferior rectus muscles. However, the ‘up’ map is orthogonal to the ‘down’ map and spans the edges of the surface where ϕ rolls over from 1 to 50. The line of maximum connection strength for the ‘up’ map is along $\phi = 1$; for ‘down’ $\phi = 26$. Based on the training described in Sect. 2.6, the maps driving the superior oblique (‘Z+’) and inferior oblique (‘Z-’) muscles were set to 1/10th of the ‘down’ and ‘up’ maps.

3.2 Saccade accuracy

In Fig. 8, we showed the result of running the model to targets located on the principle axes, on which the model was trained. We then simulated single saccades to targets in one hemifield of the eye’s field of view, with eccentricities between 6° and 14.5°. As in the training, we ran the simulation 6 times for each target, $\theta^t = (\theta_x^t, \theta_y^t, 0)$ to obtain mean saccade end-points. Fig. 10 shows saccade accuracy results for an entire hemifield in the naïve model which passed the output of SC_deep directly to SBG via the weight maps. The ratio of the magnitude of the error vector to the magnitude of the target vector is plotted using a colour map. This ratio is shown for the full, three dimensional error vector in Fig. 10(a) and for the x , y and z components in Figs. 10(b)–(c). Inspection of Fig. 10(a) shows that the end-point error is minimal along the principle axes ($\theta_x^t = 0$ or $\theta_y^t = 0$) and maximal near the 45° oblique targets (blue lines) with the end point error as high as 80% of the programmed saccade magnitude. The x component error map in Fig. 10(b) shows the same trend, mirrored about the ‘Target X’ axis, whereas the y and z component errors are, relatively, much smaller. Because the x component of the error is clearly contributing to end point errors which would not be considered ‘on target’, especially for oblique saccades, we considered the effect of the non-uniform size of the hill of activity in SC_deep.

In our model, the location, *size* and shape of activity in FEF, the basal ganglia, thalamus and superior colliculus is eccentricity dependent, in line with the retinotopic mapping stated by Ottes et al. (1986). More eccentric targets generate reduced activity, because fewer retinal neurons are excited far from the fovea. Cope et al. (2017) showed that this relationship can explain increased saccadic latencies for distal targets, resulting from reduced activity in the decision making circuitry of the basal ganglia. However, the notion that activity in superior colliculus is eccentricity-dependent conflicts with the result of Tabareau et al. (2007), who showed that an invariant hill of activity was required if this complex logarithmic weight mapping was to be used to drive a two-degree-of-freedom saccadic burst generator, and also with experimental findings, which do not show significant eccentricity dependence, at least in the burst layer (Anderson et al., 1998).

To bring our model in line with these results, whilst maintaining the eccentricity dependent activity in basal ganglia, we hypothesised that a ‘widening projection’ exists between two maps in superior colliculus. As described in Sect. 2.6, there is now experimental evidence for similar projections (Ghitani et al., 2014; Bayguinov et al., 2015) making this a plausible suggestion. Activities in one SC_deep layer remains eccentricity-dependent, with loops back to thalamus and cortex and through basal ganglia. This activity is then fed through a projection, which applies a Gaussian projection field, whose width increases with increasing stimulus eccentricity according to Eq. 28. The activity in this second SC_deep layer is then fed to the weight maps of the SBG. This model was called ‘TModel4’. TModel4 was parameterised such

834 that its horizontal and vertical error was similar—so that its equivalent of Fig. 8 showed a similar sum of
835 squares error.

836 Figs. 11(a)–(d) show the percentage errors for TModel4. First of all, note that the error magnitudes are
837 much smaller. The mean errors are smaller for every axis. The largest errors produced by the model are
838 approximately 15%, which are within the boundaries of what some authors regard as an accurate saccade
839 (McPeek and Keller, 2002; McPeek, 2006). The magnitude of the largest error vector is approximately
840 1.5°.

841 This result indicates that the exponential part of the Ottes et al. weight map from SC to the SBG cannot on
842 its own compensate for the eccentricity-dependent size of the hill of activity. The introduction of a widening
843 projection field substantially improves the mean accuracy of saccades across the field of view. We therefore
844 suggest that the transformation between retinotopically mapped activity, and eccentricity-independent
845 activity width occurs within the superior colliculus and works alongside a simple, monotonically increasing
846 weight map between SC and the SBG channels.

847 3.3 Single saccades

848 Having finalised the model by setting the weight maps, we then proceeded to exercise the model
849 (TModel4), starting with saccades to a single target; prosaccades. Fig. 12(a) shows 9 representative
850 saccades to a single target luminance. Initially, the eye had rotational state $\theta_x = \theta_y = \theta_z = 0$ with
851 its fovea directed at a fixation luminance cross (span 6°, bar width 2°) of magnitude 0.2 (in arbitrary
852 units). At a simulation time of 0.4 s, the fixation luminance was set to 0 and a target luminance cross
853 of the same dimensions as the fixation but with magnitude 0.3 was illuminated at one of the 9 different
854 locations, marked by crosses in Fig. 12(a). The resulting trajectories are plotted, with colour indicating the
855 relationship between trajectories and target crosses. The approximate end-point error is visible in this figure,
856 although the last point in each trajectory is the saccade position at 0.8 s and not the velocity-based end-point
857 described above. Figs. 12(b) and (c) show the rotational components of the blue and red trajectories in
858 Fig. 12(a) along with the target and fixation luminance values. Rotations are the eye's Euler rotational
859 components in the world frame of reference.

860 3.4 Saccade Latencies

861 To verify that our implementation of the brain model has the same functionality as that reported in Cope
862 et al. (2017), we investigated the effect on saccadic response times of: target eccentricity; and any gap or
863 overlap between fixation off-time and target on-time. We showed that the full model reproduces the ‘hockey
864 stick’ shape shown in Fig. 7 of Cope et al. (2017) and discovered in experimental data (Reulen, 1984) for
865 horizontal [Fig. 13(a)], vertical [Fig. 13(b)] and oblique saccades (not shown). The latency increases with
866 eccentricity far from the fovea because the retinotopic mapping reduces the activity in the basal ganglia for
867 more eccentric targets (see Fig. 3). Closer to the fovea, the effect of the foveal mask on the activity in FEF
868 again leads to reduced input into the basal ganglia and an increased time to achieve disinhibition in SNr.

869 Fig. 13(c) shows latencies achieved when varying the time between fixation offset and target onset. This
870 is termed the *gap condition*; and is represented by a scalar value which, if positive, refers to a gap between
871 fixation offset and target onset, and when negative, signifies an overlap, with the fixation luminance
872 persisting past the time at which the target is illuminated. A negative gap is also termed an *overlap*. Again,
873 we verify the behaviour presented in Cope et al. (2017), explained as resulting from the inhibition of
874 the cortico-thalamic loop by SNr. In the gap condition, when the fixation luminance is removed, activity
875 in STN immediately begins to decay, allowing SNr activity to reduce and thereby reducing inhibition

876 on thalamus, allowing the target luminance to build up quickly in FEF, thalamus and through the basal
877 ganglia's striatum and SNr. The shape of the curves in Fig. 13(c) matches the results in Cope et al. (2017)
878 for target luminances of 1 and 0.6; for overlaps longer than 100 ms (gap < -100 ms), the latency becomes
879 constant; the saccade is programmed whilst the fixation is present, with the target luminance inducing
880 sufficient activity in striatum to 'break through' the SNr inhibition caused by the fixation. If the target
881 luminance is reduced to 0.3, the balance is altered in favour of the fixation and the latency vs. gap becomes
882 approximately linear and equal to the overlap time plus around 100 ms.

883 Fig. 13(d) shows the effect of the dopamine parameter on saccade latencies in gap, step and overlap
884 conditions. In general, the effect of decreasing the dopamine parameter was a smooth, monotonic and
885 undramatic increase in saccade latency. However, the data for the overlap condition with a target luminance
886 which was 3 times as bright as the fixation luminance was more interesting. Here we see a transition around
887 a dopamine value of 0.7. Below this value, the basal ganglia is not able to select the target luminance until
888 the fixation is removed, reducing the excitatory drive from STN to SNr, and consequently the inhibition
889 from SNr to the thalamo-cortical loop. For the target luminance 0.6, 0.7 dopamine allows the basal ganglia
890 to select sufficiently well so that the target can build up in the thalamo-cortical loop, in spite of the fixation
891 overlap.

892 The relationship between latency and the target luminance is given in Fig. 13(e). This shows latency for a
893 100 ms gap, step and 100 ms overlap conditions for a given fixation luminance of 0.2, and a horizontally
894 located target at $\theta_y^t = -10^\circ$. For the gap condition, we see very short latencies for luminances of about
895 0.75 and above. Finally, the activity driving these express saccades is initiated by high firing rates in the
896 superficial layer of SC (SCs), which then drives activity in thalamus and through the basal ganglia. A
897 gradual transition from express saccades to reflexive saccades is observed as the contribution of the SCs
898 becomes weaker and the drive from FEF into the thalamo-cortical loop becomes necessary to elicit a
899 saccade. A similar gradual transition, albeit for higher latencies is seen for the step condition. At higher
900 target luminances, the SCs has a greater effect on the activity in the thalamo-cortical loop. However, the
901 activity in STN caused by the fixation luminance increases the latency at all luminance values compared
902 with the gap condition. The overlap condition leads to increased latencies for luminances below 2.5, but
903 meets the step condition above this value, at which the 0.2 fixation luminance appears to have a negligible
904 effect on the system.

905 3.5 Saccade sequences

906 We now present results derived from the fully parameterised and integrated model; where we took
907 advantage of the fact that it is a closed loop system. This allowed us to present sequences of target
908 luminances and allow the model to direct its fovea at the most salient target.

909 3.5.1 Out & return

910 We investigated the behaviour of the model for saccade sequences. In one experiment, we illuminated
911 a fixation cross from 0 s until 0.4 s, followed by a target at $(0, -10^\circ)$ from 0.4 s until 0.8 s. Finally, the
912 fixation was again shown from 0.8 s until the end of the simulation at 2 s. This induced a saccade to a
913 10° eccentricity, followed by a return saccade back to the null point. We noticed some irregularities in
914 the return saccades, which were accurate, but had a significant overshoot. More perplexingly, if the target
915 was switched repeatedly between 0° and 10° , second and subsequent *outward* saccades also showed this
916 overshoot. We found that the cause of these irregularities was the lack (in 'TModel4') of any mechanism to
917 reset the tonic neurons in the SBG after the first saccade. This resulted in TN activity in the left channel

918 and also in the right channel. Interestingly, this ensured that, at least for a few, consecutive out-and-return
919 saccades, the saccade accuracy was accidentally relatively good, with trajectories resembling experimental
920 data (Bahill and Stark (1979), p. 6). Had the return saccades not been so accurate, we may have noticed the
921 lack of a tonic neuron reset mechanism and corrected this oversight earlier. Such a mechanism is indeed
922 proposed and included in the connectivity of the Gancarz and Grossberg (1998) model. We implemented
923 this feature by adding an additional inhibitory input to the ‘integrator’ SBG component of TModel4, driven
924 by the contralateral EBN population, naming the new model ‘TModel5’. Now, when the eye is directed
925 towards an eccentric target which is then exchanged with a target at the null point, the EBN activity toward
926 the null point will tend to extinguish the TN activity which was holding the eye at the eccentric position.
927 We verified that none of the single saccade results were affected by this modification.

928 Fig. 14 shows the outward and return trajectories produced by the experiment with the TN reset mecha-
929 nism. Panel (a) shows the x and y rotation trajectory; panel (b) shows individual rotational components of
930 the eye. Fig. 14(c) shows out and return trajectories for three other saccade targets; horizontal, vertical and
931 oblique. The trajectories have characteristic shapes and also show some stochastic variation caused by the
932 noise in the model [see dashed trajectories in Fig. 14(a)].

933 The return trajectories (magenta lines) showed a distinctly different form from the outward trajectories.
934 They overshot their destination (the null point) significantly. This resulted from the removal of the TN
935 activity which was holding the eye at the eccentric target location. Removal of this activity, and thus the
936 static force exerted by the corresponding extraocular muscle, meant that the eye was subject both to a new
937 muscular force towards the null point *alongside* the restorative spring force of the lengthened rectus muscle.
938 This stands as a shortcoming of the model.

939 3.5.2 Double steps

940 In another experiment, we probed the response of the model to double step stimuli of the type described
941 in Becker and Jürgens (1979). In that work, the response of human subjects was investigated when shown
942 stimuli at 15° and 30° eccentricity with variable delay between the stimuli. If the smaller eccentricity
943 stimulus was shown first, followed by the more distal on the same side of the field of view, this was called
944 a ‘staircase’ presentation. We carried out a ‘staircase’ presentation, shown in Fig. 15, where our small
945 eccentricity luminance was at 8° and our more distal luminance was at 12° (both to the right of centre).
946 The stimuli could not be presented at 15° and 30° to match the experiment, because 30° saccades were
947 outside the range of the model.

948 We found that there was a critical time delay between the luminances of about 30 ms. If they were
949 presented with a delay smaller than this value, then a single, slightly hypermetric saccade was made. This
950 response type is called a *final angle response*. A delay greater than 30 ms between the stimuli would lead to
951 double step saccades (a so-called *initial angle response*), with the first saccade arriving at 8° (though with
952 greater variability than normal), and a second saccade being made to a location hypometric of 12° after a
953 pause of about 240 ms. Fig. 15(a) shows the mean trajectories from 5 simulations of the staircase doublestep
954 presentation alongside the result for a single saccade to the final angle of 12° . Dash-dot lines show ± 1
955 standard deviation about the mean. The corresponding trajectories are shown in Fig. 15(b).

956 Inspection of the activity maps in FEF and SC_deep (not shown) indicates that when the 8° target
957 is illuminated for 30 ms or more, the activity associated with this target angle is able to dominate the
958 activity, hence the execution of a reasonably accurate saccade. The inhibitory feedback from the SBG then
959 extinguishes activity in FEF, thalamus and SC, which means that a full 200 ms or more is required to allow
960 activity in these populations to build up again in order to make the smaller saccade from 8° to 12° . This is

961 in contrast to experimental findings in which the corrective second saccade is often executed *more quickly*
962 than if it were programmed on its own (Becker and Jürgens, 1979).

4 DISCUSSION

963 The aim of this study was to demonstrate the importance of modelling neurological systems *in concert with*
964 the biomechanical systems with which they have evolved. We hypothesised that by combining existing
965 neurophysiological models with an accurate model of a musculo-skeletal system, and then closing the
966 ‘agent-environment-agent’ loop by allowing the movements of the virtual muscles to modulate sensory
967 feedback to the brain model, shortcomings in the constituent models would be revealed, leading to new
968 knowledge.

969 To demonstrate the validity of this closed-loop approach, we built an integrated model and then identified
970 the modifications which were necessary to give it the ability to make accurate movements under one type
971 of stimulus. We then examined its behaviour with other stimuli. We chose the oculomotor model as a basis
972 for this study because it has only three degrees of freedom, making it one of the simplest musculo-skeletal
973 systems. Furthermore, eye movements fall into several well-defined categories, each being controlled by
974 separate brain circuits, we were therefore justified in modelling a system which produced only saccadic
975 eye movements. Nevertheless, we are aware that we did not create a complete model of the system; no
976 treatment of the cerebellum was attempted, justified because cerebellum appears to have only a minor
977 effect on saccade accuracy (Dean and Porrill, 2008), probably correcting for slow to medium timescale
978 changes in the physical dynamics of the eyeball (Dean et al., 1994).

979 To summarise our model integration: We combined the Cope-Chambers model (Cope et al., 2017) with a
980 saccadic burst generator model based on the work of Gancarz and Grossberg (1998), using this to drive the
981 input of a new biomechanical eye model. To achieve the spatial transformation from the retinotopic maps of
982 the Cope-Chambers model to the six ‘muscle channel’ inputs for the saccadic burst generator, we used the
983 mapping of Ottes et al. (1986) to produce parameterised weight maps along with an empirically discovered
984 synergy for the torsional weight maps. We introduced an additional transformation to the brain model to
985 achieve invariant sized hills of activity in superior colliculus to fulfil the invariant integral hypothesis of
986 Tabareau et al. (2007). We closed the loop using a software component which transformed a view of a
987 world containing luminous cross shapes into the eye’s frame of reference, given its instantaneous rotational
988 state. This component also computed the inverse of the mapping from Ottes et al. (1986) to project the view
989 retinotopically into the brain model. This paper serves to describe how we achieved the integration in order
990 to test our hypothesis, and we intend that the material and methods section, along with the model code
991 itself, will help others to carry out similar studies. We will discuss what can be learned from an integrated
992 model of a combined brain and biomechanical system, using our oculomotor system as an example and
993 then consider how this study compares with other modelling and robotic studies of closed-loop systems.

994 Our integration approach revealed three ways in which this model fails to provide a full understanding
995 of the saccadic system. In each case, the issue is made clear *as a result of the integration*. This is not to
996 say that other approaches may not also reveal shortcomings; we will see that one of our cases has been
997 independently identified (Groh, 2011).

998 4.1 The need for a widening projection field

999 The original combination of the Cope-Chambers model with the theoretical weight maps of Ottes et al.
1000 (1986) and Tabareau et al. (2007) resulted in a model which was able to produce accurate saccades only

1001 along the principle rotational axes (Fig. 10). Thus, *the integration of the models* suggested that an additional
1002 layer was required to achieve accurate saccades for oblique, as well as for horizontal and vertical saccades.
1003 Although the *need* for an invariant integral is discussed in Tabareau et al. (2007) as resulting from their
1004 theoretical study, the mechanism by which such an invariant Gaussian hill is generated is not. By combining
1005 the models, we were forced to consider this mechanism, and hypothesised that a widening projection field
1006 would be a candidate mechanism. The results of Fig. 11 indicate that a substantial improvement in accuracy
1007 is indeed achieved by this new mechanism.

1008 4.2 Saccades from non-null starting positions

1009 The implementation of a biologically accurate model of the eye, and the closed-loop nature of the model
1010 makes it very natural to consider how the model will behave when making saccades from arbitrary starting
1011 positions, or how it would respond to a sequence of stimuli. This was the motivation for the out-and-return
1012 experiment (Fig. 14) as well as for the double step experiment (Fig. 15). We found that return saccades were
1013 substantially affected by the biomechanics of the eye, as the brain and brainstem model had no mechanism
1014 to account for the position-dependent restoring forces applied by the eye. This question has been addressed
1015 by other authors; Groh (2011) investigates the effect of initial eye position on stimulated saccades and finds
1016 a need for the signal in superior colliculus to be modulated by an eye position signal. Ling et al. (2007)
1017 shows the existence of a position dependent firing rate offset in abducens neurons. Though we will not
1018 speculate here on the mechanism by which return saccades may be made accurate whilst also resetting
1019 the activity of tonic neurons in the SBG, it is interesting that in the model in which we omitted to reset
1020 TN activity (TModel4), we obtained relatively accurate out-and-return saccades which closely resembled
1021 experimental data. We suggest that residual activity in TN populations may offer an explanation for how
1022 the restorative force exerted by the elastic oculomotor muscles is compensated for. A comparison of this
1023 idea with that of Groh (2011) (that there is a modulation, from a brainstem signal, of the SC readout) would
1024 make a subject for a future study. Although these existing studies have highlighted this issue, the inaccurate
1025 return saccades which the model makes from eccentric starting positions provide a clear example of the
1026 way in which integrating known models into a closed-loop system can highlight deficiencies in the model.

1027 4.3 Inhibitory feedback from saccadic burst generator to brain

1028 The third issue raised by the integration of the component models of the saccadic system has, like
1029 the return saccades, to do with resetting activity. In this case, rather than the reset of activity in the TN
1030 population in the brainstem, it is the question of how the activity in the *brain* model should be reset after
1031 each saccade. When a target luminance is projected onto the World population in the model, this induces
1032 activity which ‘reverberates’ in loops through FEF, basal ganglia, SC and thalamus. The brainstem contains
1033 a mechanism to limit the timescale of a saccade (inhibitory feedback from EBN, via IBN to LLBN; see
1034 Fig. 4). However, if the activity in SC is not reset, then following the completion of the first saccade, a
1035 series of subsequent ‘staircase’ saccades will be executed. There needs to be a mechanism to extinguish
1036 activity in SC, but also in FEF and thalamus, as activity in either of these populations can build up and
1037 eventually cause repeat activity in SC and another saccade. We added hypothetical inhibitory feedback
1038 connections to our model, such that the IBN populations in the SBG would inhibit activity in FEF, thalamus
1039 and SC_deep (Fig. 4), preventing the occurrence of staircase saccades.

1040 An examination of the behaviour of the model when presented with ‘double-step stimuli’ reveals a
1041 problem with our inhibitory feedback connections. We found that when double-step stimuli were presented
1042 (where an initial target at 8° was replaced with a 12° target after 30 or 40 ms) and a double saccade was
1043 made [Fig. 15(a), black lines] the second saccade latency was *longer* even than the initial saccade. This

1044 contrasts with Becker and Jürgens (1979) who find that second, corrective saccades occur with *shorter*
1045 latencies. This suggests that the inhibitory reset signal implemented in this model is too strong or has the
1046 wrong timescales. This issue highlights the fact that connections *between* component models are quite as
1047 important as the connections within each model.

1048 There is some evidence for an inhibitory projection to SC from the brainstem. Corvisier and Hardy
1049 (1991) offer evidence for a projection from the propositus hypoglossi nucleus. This lies upstream from
1050 motoneurons and (in primates) encodes eye velocity (Dale and Cullen, 2013), rather than head movement
1051 velocity. Although the propositus hypoglossi does not lie in exactly the same functional location as our IBN
1052 population (instead it sits between TN and MN), it offers a possible inhibitory feedback signal proportional
1053 to eye velocity and may help to reduce activity in SC post-saccade. Alternatively, it is possible that activity
1054 in FEF and thalamus are reset via a ‘timed signal’. Feasibly, after activity in FEF exceeds a threshold, an
1055 internal, inhibitory feedback signal could be activated. This inhibition should have a timescale of sufficient
1056 duration to reduce activity in FEF, thalamus and, via an increase in inhibitory output from SNr, also in
1057 SC. Indeed, the cortical microcircuit contains a variety of morphologically distinct GABAergic neurons
1058 (Douglas and Martin, 2004) which could fulfil this functionality. A similar mechanism would then be
1059 required in SC, to reset activity generated by direct excitation via the retinal-collicular pathway which
1060 generates express saccades. Again, SC is a multi-layered structure, containing GABAergic interneurons
1061 (Muñoz and Istvan, 1998; Meredith and Ramoa, 1998; Helms et al., 2004; Sooksawate et al., 2011) and
1062 there is mounting evidence that saccade dynamics are generated within SC (Kaneda et al., 2008; Goossens
1063 and van Opstal, 2012; Bayguinov et al., 2015). Thus, a more complex treatment of the SC and FEF regions
1064 in the model may well obviate the need for inhibitory feedback from brainstem to SC, FEF and thalamus.

1065 Considering whether a feedback connection, or internal, recurrent inhibition is responsible for activity-
1066 reset in the brain model raises a more general question about modelling the central nervous system. We
1067 should consider whether inaccuracies within one part of the model may propagate errors through the
1068 closed-loop system that cannot be counteracted by another part of the simulation. There is no way to know,
1069 from integrating sub-systems, which properties hold true, and which are false. However, by integrating
1070 models and examining the behaviour of the combined model, we are presented with the right questions to
1071 ask of the model and the experimental data. In the case of activity-reset, this is to re-assess whether there
1072 exists inhibitory feedback from brainstem to the SC and FEF regions, and to find out how an integrated
1073 model with self-regulatory mechanisms in SC and FEF may perform.

1074 The omission of the cerebellum will not have escaped the reader’s notice. Whilst many of the nuclei
1075 known to be involved in the production of saccadic eye movements are incorporated within the model,
1076 the cerebellum is not. The cerebellum is known to play an important rôle in saccade programming (Dean
1077 et al., 1994; Schweighofer et al., 1996; Quaia et al., 2000; Kleine, 2003). It may be able to completely
1078 replace the functionality of the colliculus when lesioned (Aizawa and Wurtz, 1998; Lefèvre et al., 1998).
1079 However, this rôle is typically considered to be one of accuracy tuning (Barash et al., 1999; Dean et al.,
1080 1994); operating as an additive model. Furthermore, saccades made by individuals with cerebellar ataxias
1081 perform with only moderate loss of saccade accuracy (Barash et al., 1999; Federighi et al., 2011). Because
1082 we did not address learning in our model, and because our aim was to demonstrate the utility of integrating
1083 brain with biomechanics in order to highlight deficiencies, we considered the omission of the cerebellar
1084 nuclei acceptable in the present work.

1085 We have not addressed the question of saccade duration in this paper. Saccade duration is of interest in
1086 models which produce two (or three) dimensional saccades, because the dynamics of a saccade follow well
1087 known relationships with the saccade eccentricity, regardless of the saccade angle. This causes a problem for

models (such as the present one) for which some of the dynamic behaviour is generated within orthogonal components. For example, saccade duration increases with target eccentricity. A 10° eccentricity oblique (45° up and right) saccade is composed (approximately) of a 7° upwards component and a 7° rightwards component. If the component based model is responsible for the dynamics, then the 10° oblique saccade would be expected to have the dynamics of a 7° up or 7° right saccade. This is not found in practice, and the components are said to have been stretched, hence the name for this effect ‘component stretching’. The Gancarz and Grossberg (1998) model is reported to take account of the component stretching effect via the OPN neuron population. We did not find this effect in our implementation of the model; the duration of oblique saccades at a given eccentricity was always substantially different from the duration of the corresponding purely vertical or horizontal saccade. Because there is a somewhat complicated interplay between the dynamics of the superior colliculus driving the dynamic system of the SBG, we feel this is outside the scope of the current work and a subject for a future paper.

4.4 Comparison with other studies

We have called this closed-loop, biomimetic modelling approach *computational neurobehaviour*, in which a complete, behaving model is constructed, with attention paid to the biological accuracy of each brain and biomechanical sub-system. We are by no means the first researchers to consider this interaction between brain and biomechanics. Integrative approaches to motor control have been referred to as *neuromechanics* by some authors (Nishikawa et al., 2007). This field appears to have developed from detailed and low level studies of the mechanics of muscle control systems, focussing on the neural systems ‘closest’ to the muscle (Chiel et al., 2009). It is evident that a recognition of the importance of sensory input to these systems has evolved within this field. Indeed, Edwards (2010) specifically reviews closed-loop, *neuromechanical simulations* of behaviour in three organisms; fly, locust and cat. The term neuromechanical simulation (Pearson et al., 2006; Edwards, 2010) is analogous to our computational neurobehaviour, although it does not emphasise the important *behavioural* aspect of the works.

There also exist many closed-loop *robotic* systems which receive sensory input from the world, process that input and generate behaviour by activating motor systems (Yu et al., 2004; Fend et al., 2004; Pearson et al., 2007). We now consider whether robotic systems which model biological components *in hardware* could fall within our new category. Using a number of examples, we will attempt to illustrate what we mean by computational neurobehaviour. We’ll consider which examples fall into the new category and which are covered by other fields of robotics or computational neuroscience.

Pearson et al. (2007) describe a wheeled robot which has a biomimetic whisker sensory system, along with a biomimetic neural system imitating the operation of the rat’s sensory processing and controlling the movement of the robot. Fend et al. (2004) is a similar, wheeled, whiskered robot, with a repertoire of three behaviours organised in a subsumption architecture. In both robots, actions that are selected within the brain model drive a non-biologically accurate motor control algorithm to achieve rotational and translational movements. Although both have sensory and processing systems which are guided by biology, the non-biological motor control stage prevents us from considering these as being studies of computational neurobehaviour. Instead, we would refer to these as *embodied models*, as described in Bolado-Gomez and Gurney (2013), a study in which the learning behaviour of a biomimetic ‘core’ model is embedded within an engineered ‘architecture’ (a wheeled robot) which closes the agent-environment loop. Yu et al. (2004) report on a biomimetic fish robot, whose motor system closely resembles that of the real fish. The robot is able to operate in a closed-loop mode, where sensory input is provided to the non-biomimetic control algorithms from overhead cameras, but its control system is also able to operate in open-loop mode. Neither

1131 the control system, nor the sensory system are biologically accurate and we would not describe this study
1132 as computational neurobehaviour. Nevertheless, the biomechanically accurate motor system they describe
1133 has the potential to form part of a computational neurobehavioural study of swimming behaviour in the
1134 fish, if it were combined in a loop with suitable sensory input and sensory processing models. Knips et al.
1135 (2017) is a report of a reach-and-grasp robot arm controlled via a dynamic neural field brain model. The
1136 sensory input for this system—its ‘eyes’—is a Microsoft Kinect sensor; it also has somatosensory feedback
1137 from the fingers of the robot’s hand. The neural field ‘brain’ controls the seven degrees of freedom of
1138 the arm to carry out the reach-and-grasp action. While this robot has closed-loop control and is clearly
1139 inspired by biology, it remains a study of robotics and of the improvement of the control of the robot’s
1140 reach-and-grasp function, rather than a study which aims to learn more about the biology of a primate arm.
1141 For this reason, we would describe the study of Knips et al. (2017) as an embodied model.

1142 To summarise, in most closed-loop robotic studies which incorporate neuromimetic models, the hardware
1143 forms an ‘engineered surround architecture’ allowing for the examination of the behaviour of the embodied
1144 model. However, suitably *biomimetic* hardware such as the fish in Yu et al. (2004) would not be excluded
1145 from computational neurobehavioural studies, especially if movement is by biomimetic muscle actuators
1146 (Wilson et al., 2016; OHalloran et al., 2008).

1147 Modern programming platforms, often originating from the computer game industry, make it relatively
1148 easy to model a virtual environment. Consequently, an increasing number of studies into robotic or
1149 neuromimetic control are carried out with virtual robots operating within a virtual environment. This
1150 approach is taken in the studies described in Edwards (2010). Dickson et al. (2006) describes an integrated
1151 model of Drosophila flight in which visual input is processed by an algorithmic (that is, non-neural) ‘brain’
1152 to control a biomechanically accurate representation of the fly. As the virtual fly traverses its environment,
1153 its visual input updates, closing the loop of the simulation. Cope et al. (2016b) is a recent study which
1154 omits the biomechanically accurate component of the model but could provide the biologically plausible
1155 brain to make a computational neurobehavioural fly model. Cofer et al. (2010a) use an environment called
1156 AnimatLab (Cofer et al., 2010b) to simulate the locust’s jumping mechanism in an open-loop, software-only
1157 investigation. As this appears to be a feed-forward model without sensory feedback, we would describe
1158 it as an input-assumption model. N’Guyen et al. (2014) and Thurat et al. (2015) are two studies of the
1159 oculomotor system which model sensory input, neural control *and* motor output in software. These studies
1160 fall outside the remit of computational neurobehaviour only because they omit to close the sensory loop.
1161 DeWolf et al. (2016) describes a reach model comprising a simplified virtual arm (with fewer degrees of
1162 freedom than a primate arm), and a biologically inspired brain model. This model also omits to close the
1163 sensory feedback loop and we consider it a computational neuroscience study of a (virtually) embodied
1164 model.

1165 There are also experimental closed-loop approaches to understanding sensorimotor control. Ejaz et al.
1166 (2013) places a fly in a fixed position, and couples it with a free-to-move robot. The sensory input collected
1167 by the robot is projected onto the eyes of the fly, and activity from a selected neuron in the fly’s brain
1168 is used to drive a control system for the robot’s movements. This allows the experimenters to study the
1169 behaviour of the fly’s brain operating in a closed-loop condition that is more natural than the open-loop
1170 condition that many other experimental techniques mandate. The results from closed-loop experiments will
1171 undoubtedly inform future neurobehavioural models.

1172 Thus, while there are many models that close the agent-environment loop and display partial biological
1173 plausibility, the biomimetic features are usually confined to a sub-system of the entire model. This leads us
1174 to formalise a definition of computational neurobehaviour as: *The study of biological sensory-motor system*

1175 behaviour using biologically accurate models of sensory input, brain and motor sub-systems operating
1176 in a closed-loop. We believe our oculomotor model is one of the first such models using this approach
1177 and shares many features with that of Arena et al. (2017) which describes a robotic insect system based
1178 on the fly species *Drosophila Melanogaster*. It has biomimetic insect legs implemented in a virtual robot
1179 and a neuromimetic brain. Closing the loop is a visual sensory input system which is able to determine
1180 the distance to an on-coming obstacle and the obstacle's height. The authors demonstrate that the virtual
1181 robot is able to learn to climb in a realistic manner and suggest it may be compared with experimental data
1182 from future Drosophila experiments addressing obstacle climbing and learning. The visual system is not
1183 described in detail, but if it is modelled in a biologically plausible manner, then this work may reasonably
1184 be described as a computational neurobehaviour study, contemporaneous with our own.

DISCLOSURE/CONFLICT-OF-INTEREST STATEMENT

1185 The authors declare that the research was conducted in the absence of any commercial or financial
1186 relationships that could be construed as a potential conflict of interest.

AUTHOR CONTRIBUTIONS

1187 SJ, AB and AC implemented existing parts of the model in SpineML. AB developed the saccade generator
1188 brainstem model. SJ performed the technical and scientific integration of the biomechanical eye. CP and
1189 KM developed the biomechanical eye model. SJ wrote the manuscript; SA, AB, KG and KM contributed
1190 to the manuscript. KG conceived the project.

ACKNOWLEDGEMENTS

1191 *Funding:* European Union FP7 Grant 610391 ‘NoTremor’.

SUPPLEMENTAL DATA

1192 The model specification, results and all code required to reproduce the results of this work are available at:
1193 https://github.com/ABRG-Models/OMM_NeuroMuscular

REFERENCES

- 1194 Aizawa, H. and Wurtz, R. H. (1998). Reversible inactivation of monkey superior colliculus. I. Curvature of
1195 saccadic trajectory. *Journal of neurophysiology* 79, 2082–2096
1196 Alex Cope and Paul Richmond (2014). SpineML. RRID: SCR_015641
1197 Anderson, R. W., Keller, E. L., Gandhi, N. J., and Das, S. (1998). Two-dimensional saccade-related
1198 population activity in superior colliculus in monkey. *Journal of Neurophysiology* 80, 798–817
1199 Arai, K., Keller, E., and Edelman, J. (1994). Two-dimensional neural network model of the primate
1200 saccadic system. *Neural Networks* 7, 1115. doi:10.1016/S0893-6080(05)80162-5
1201 Arai, K. and Keller, E. L. (2005). A model of the saccade-generating system that accounts for trajectory
1202 variations produced by competing visual stimuli. *Biological cybernetics* 92, 21–37. doi:10.1007/
1203 s00422-004-0526-y
1204 Arena, E., Arena, P., Strauss, R., and Patané, L. (2017). Motor-Skill Learning in an Insect Inspired
1205 Neuro-Computational Control System. *Frontiers in Neurorobotics* 11. doi:10.3389/fnbot.2017.00012

- 1206 Bahill, A. T. and Stark, L. (1979). The trajectories of saccadic eye movements. *Scientific American* 240,
1207 108–117
- 1208 Barash, S., Melikyan, A., Sivakov, A., Zhang, M., Glickstein, M., and Thier, P. (1999). Saccadic dysmetria
1209 and adaptation after lesions of the cerebellar cortex. *Journal of Neuroscience* 19, 10931–10939
- 1210 Bayguinov, P. O., Ghitani, N., Jackson, M. B., and Basso, M. A. (2015). A Hard-Wired Priority Map
1211 in the Superior Colliculus Shaped by Asymmetric Inhibitory Circuitry. *Journal of Neurophysiology*
1212 doi:10.1152/jn.00144.2015
- 1213 Becker, W. and Jürgens, R. (1979). An analysis of the saccadic system by means of double step stimuli.
1214 *Vision Research* 19, 967–983. doi:10.1016/0042-6989(79)90222-0
- 1215 Bevan, M. D. and Wilson, C. J. (1999). Mechanisms underlying spontaneous oscillation and rhythmic
1216 firing in rat subthalamic neurons. *The Journal of neuroscience : the official journal of the Society for
1217 Neuroscience* 19, 7617–28
- 1218 Blenkinsop, A., Anderson, S., and Gurney, K. (2017). Frequency and function in the basal ganglia: the
1219 origins of beta and gamma band activity. *The Journal of Physiology* doi:10.1113/JP273760
- 1220 Bogacz, R. and Gurney, K. (2007). The basal ganglia and cortex implement optimal decision making
1221 between alternative actions. *Neural Computation* 19, 442–477. doi:10.1162/neco.2007.19.2.442
- 1222 Bolado-Gomez, R. and Gurney, K. (2013). A biologically plausible embodied model of action discovery.
1223 *Frontiers in Neurorobotics* 7. doi:10.3389/fnbot.2013.00004
- 1224 Bolam, J., Hanley, J., Booth, P., and Bevan, M. (2000). Synaptic organisation of the basal ganglia. *Journal
1225 of Anatomy* 196, 527–542
- 1226 Brown, P., Oliviero, A., Mazzone, P., Insola, A., Tonali, P., and Di Lazzaro, V. (2001). Dopamine
1227 Dependency of Oscillations between Subthalamic Nucleus and Pallidum in Parkinson's Disease. *J.
1228 Neurosci.* 21, 1033–1038
- 1229 Bruce, C. J. and Goldberg, M. E. (1985). Primate frontal eye fields. I. Single neurons discharging before
1230 saccades. *Journal of Neurophysiology* 53, 603–635
- 1231 Casteau, S. and Vitu, F. (2012). On the effect of remote and proximal distractors on saccadic behavior: A
1232 challenge to neural-field models. *Journal of vision* 12, 14
- 1233 Chambers, J. M., Gurney, K., Humphries, M., and Prescott, A. (2012). Mechanisms of choice in the
1234 primate brain: a quick look at positive feedback. In *Modelling Natural Action Selection* (Cambridge
1235 University Press). 390–420
- 1236 Chen, L. L. and Wise, S. P. (1995). Supplementary eye field contrasted with the frontal eye field during
1237 acquisition of conditional oculomotor associations. *Journal of Neurophysiology* 73, 1122–1134
- 1238 Chevalier, G. and Deniau, J. M. (1990). Disinhibition as a basic process in the expression of striatal
1239 functions. *Trends in Neurosciences* 13, 277–280
- 1240 Chiel, H. J., Ting, L. H., Ekeberg, Ö, and Hartmann, M. J. Z. (2009). The Brain in Its Body: Motor Control
1241 and Sensing in a Biomechanical Context. *Journal of Neuroscience* 29, 12807–12814. doi:10.1523/
1242 JNEUROSCI.3338-09.2009
- 1243 Cofer, D., Cymbalyuk, G., Heitler, W. J., and Edwards, D. H. (2010a). Neuromechanical simulation of the
1244 locust jump. *The Journal of Experimental Biology* 213, 1060. doi:10.1242/jeb.034678
- 1245 Cofer, D., Cymbalyuk, G., Reid, J., Zhu, Y., Heitler, W. J., and Edwards, D. H. (2010b). AnimatLab: A 3d
1246 graphics environment for neuromechanical simulations. *Journal of Neuroscience Methods* 187, 280–288.
1247 doi:10.1016/j.jneumeth.2010.01.005
- 1248 Cohen, J. Y., Heitz, R. P., Woodman, G. F., and Schall, J. D. (2009). Neural basis of the set-size effect in
1249 frontal eye field: timing of attention during visual search. *Journal of Neurophysiology* 101, 1699–1704.
1250 doi:10.1152/jn.00035.2009

- 1251 Cope, A., Chambers, J. M., Prescott, T. J., and Gurney, K. N. (2017). Basal Ganglia Control Of
1252 Reflexive Saccades: A Computational Model Integrating Physiology Anatomy And Behaviour. *bioRxiv*
1253 doi:10.1101/135251
- 1254 Cope, A. and Gurney, K. N. (2011). A biologically based model of active vision. In *Proceedings of*
1255 *AISB'11 - Architectures for Active Vision*, eds. S. O'Keefe, Kazakov, D., and Tsoulas, D. (York, UK),
1256 13–20
- 1257 Cope, A. J. and James, S. S. (2015). SpineML_2_brahms. RRID: SCR_015640
- 1258 Cope, A. J., Richmond, P., and Allerton, D. (2014). The SpineML toolchain: enabling computational neu-
1259 roscience through flexible tools for creating, sharing, and simulating neural models. *BMC Neuroscience*
1260 15, P224
- 1261 Cope, A. J., Richmond, P., and James, S. S. (2015). SpineCreator. RRID: SCR_015637
- 1262 Cope, A. J., Richmond, P., James, S. S., Gurney, K., and Allerton, D. J. (2016a). SpineCreator: a
1263 Graphical User Interface for the Creation of Layered Neural Models. *Neuroinformatics* doi:10.1007/
1264 s12021-016-9311-z
- 1265 Cope, A. J., Sabo, C., Gurney, K., Vasilaki, E., and Marshall, J. A. R. (2016b). A Model for an Angular
1266 Velocity-Tuned Motion Detector Accounting for Deviations in the Corridor-Centering Response of the
1267 Bee. *PLOS Computational Biology* 12, e1004887. doi:10.1371/journal.pcbi.1004887
- 1268 Corvisier, J. and Hardy, O. (1991). Possible excitatory and inhibitory feedback to the superior colliculus: a
1269 combined retrograde and immunocytochemical study in the prepositus hypoglossi nucleus of the guinea
1270 pig. *Neuroscience Research* 12, 486–502. doi:10.1016/S0168-0102(09)80002-3
- 1271 Dale, A. and Cullen, K. E. (2013). The nucleus prepositus predominantly outputs eye movement-
1272 related information during passive and active self-motion. *Journal of Neurophysiology* 109, 1900.
1273 doi:10.1152/jn.00788.2012
- 1274 Daniel, P. M. and Whitteridge, D. (1961). The representation of the visual field on the cerebral cortex in
1275 monkeys. *The Journal of Physiology* 159, 203–221. doi:10.1113/jphysiol.1961.sp006803
- 1276 Dean, P. (1995). Modelling the role of the cerebellar fastigial nuclei in producing accurate saccades: the
1277 importance of burst timing. *Neuroscience* 68, 1059–1077
- 1278 Dean, P., Mayhew, J. E., and Langdon, P. (1994). Learning and maintaining saccadic accuracy: a model of
1279 brainstemcerebellar interactions. *Journal of Cognitive Neuroscience* 6, 117–138
- 1280 Dean, P. and Porrill, J. (2008). Adaptive filter models of the cerebellum: computational analysis. *Cerebellum*
1281 7, 567–571
- 1282 Delgado, A., Sierra, A., Querejeta, E., Valdiosera, R., and Aceves, J. (1999). Inhibitory control of the
1283 GABAergic transmission in the rat neostriatum by D2 dopamine receptors. *Neuroscience* 95, 1043–1048.
1284 doi:10.1016/S0306-4522(99)00495-9
- 1285 DeLong, M., Crutcher, M. D., and Georgopoulos, A. (1985). Primate globus pallidus and subthalamic
1286 nucleus: functional organization. *Journal of Neurphysiology* 53, 530–543
- 1287 Deubel, H. and Schneider, W. X. (1996). Saccade target selection and object recognition: Evidence for a
1288 common attentional mechanism. *Vision Research* 36, 1827–1837. doi:10.1016/0042-6989(95)00294-4
- 1289 DeWolf, T., Stewart, T. C., Slotine, J.-J., and Eliasmith, C. (2016). A spiking neural model of adaptive arm
1290 control. *Proceedings of the Royal Society B: Biological Sciences* 283, 20162134. doi:10.1098/rspb.2016.
1291 2134
- 1292 Dickson, W., Straw, A., Poelma, C., and Dickinson, M. (2006). An Integrative Model of Insect Flight
1293 Control (Invited) (American Institute of Aeronautics and Astronautics). doi:10.2514/6.2006-34
- 1294 Dorris, M. C., Paré, M., and Munoz, D. P. (1997). Neuronal Activity in Monkey Superior Colliculus
1295 Related to the Initiation of Saccadic Eye Movements. *The Journal of Neuroscience* 17, 8566

- 1296 Douglas, R. J. and Martin, K. A. C. (2004). Neuronal Circuits of the Neocortex. *Annual Review of*
1297 *Neuroscience* 27, 419–451. doi:10.1146/annurev.neuro.27.070203.144152
- 1298 Edelman, J. A. and Keller, E. L. (1996). Activity of visuomotor burst neurons in the superior colliculus
1299 accompanying express saccades. *Journal of Neurophysiology* 76, 908
- 1300 Edwards, D. H. (2010). Neuromechanical Simulation. *Frontiers in Behavioral Neuroscience* 4. doi:10.
1301 3389/fnbeh.2010.00040
- 1302 Ejaz, N., Krapp, H. G., and Tanaka, R. J. (2013). Closed-loop response properties of a visual interneuron
1303 involved in fly optomotor control. *Frontiers in Neural Circuits* 7. doi:10.3389/fncir.2013.00050
- 1304 Federighi, P., Cevenini, G., Dotti, M. T., Rosini, F., Pretegiani, E., Federico, A., et al. (2011). Differences
1305 in saccade dynamics between spinocerebellar atrophy 2 and late-onset cerebellar ataxias. *Brain* 134,
1306 879–891. doi:10.1093/brain/awr009
- 1307 Fend, M., Bovet, S., and Hafner, V. (2004). The artificial mouse-a robot with whiskers and vision.
1308 *Proceedings of the 35th International Symposium on Robotics, Paris, 2004.*, 1–6
- 1309 Fuchs, A. and Luschei, E. (1970). Firing patterns of abducens neurons of alert monkeys in relationship to
1310 horizontal eye movement. *Journal of Neurophysiology* 33, 382–392
- 1311 Funahashi, S., Chafee, M. V., and Goldman-Rakic, P. S. (1993). Prefrontal neuronal activity in rhesus
1312 monkeys performing a delayed anti-saccade task. *Nature* 365, 753
- 1313 Galvan, A. and Wichmann, T. (2008). Pathophysiology of Parkinsonism. *Clinical Neurophysiology* 119,
1314 1459–1474. doi:10.1016/j.clinph.2008.03.017
- 1315 Gancarz, G. and Grossberg, S. (1998). A neural model of the saccade generator in the reticular formation.
1316 *Neural Networks* 11, 1159–1174. doi:10.1016/S0893-6080(98)00096-3
- 1317 Gaymard, B., Ploner, C. J., Rivaud, S., Vermersch, A. I., and Pierrot-Deseilligny, C. (1998). Cortical
1318 control of saccades. *Experimental Brain Research* 123, 159–163. doi:10.1007/s002210050557
- 1319 Gerfen, C. R., Engbar, T. M., Mahan, L. C., Susel, Z., Chase, T. N., Monsma, F. J., et al. (1990). D1 and
1320 D2 dopamine receptor regulated gene-expression of striatonigral and striatopallidal neurons. *Science*
1321 250, 1429–1432
- 1322 Ghitani, N., Bayguinov, P. O., Vokoun, C. R., McMahon, S., Jackson, M. B., and Basso, M. A. (2014).
1323 Excitatory Synaptic Feedback from the Motor Layer to the Sensory Layers of the Superior Colliculus.
1324 *The Journal of Neuroscience* 34, 6822–6833. doi:10.1523/JNEUROSCI.3137-13.2014
- 1325 Gian G. Mascetti and Jorge R. Arriagada (1981). Tectotectal interactions through the commissure of the
1326 superior colliculi. An electrophysiological study. *Experimental Neurology* 71, 122–133
- 1327 Girard, B. and Berthoz, A. (2005). From brainstem to cortex: Computational models of saccade generation
1328 circuitry. *Progress in Neurobiology* 77, 215–251. doi:10.1016/j.pneurobio.2005.11.001
- 1329 Goldberg, M. E. and Wurtz, R. H. (1972). Activity of superior colliculus in behaving monkey. I. Visual
1330 receptive fields of single neurons. *J Neurophysiol* 35, 542–559
- 1331 Gonon, F. (1997). Prolonged and extrasynaptic excitatory action of dopamine mediated by D1 receptors in
1332 the rat striatum in vivo. *The Journal of neuroscience : the official journal of the Society for Neuroscience*
1333 17, 5972–8
- 1334 Goossens, H. (2006). Dynamic Ensemble Coding of Saccades in the Monkey Superior Colliculus. *Journal*
1335 *of Neurophysiology* 95, 2326–2341. doi:10.1152/jn.00889.2005
- 1336 Goossens, H. and van Opstal, A. J. (2012). Optimal control of saccades by spatial-temporal activity patterns
1337 in the monkey superior colliculus. *PLoS computational biology* 8, e1002508
- 1338 Grantyn, A., Brandi, A.-M., Dubayle, D., Graf, W., Ugolini, G., Hadjidakis, K., et al. (2002).
1339 Density gradients of trans-synaptically labeled collicular neurons after injections of rabies virus in the

- 1340 lateral rectus muscle of the rhesus monkey. *The Journal of Comparative Neurology* 451, 346–361.
1341 doi:10.1002/cne.10353
- 1342 Groh, J. M. (2001). Converting neural signals from place codes to rate codes. *Biological cybernetics* 85,
1343 159–165
- 1344 Groh, J. M. (2011). Effects of Initial Eye Position on Saccades Evoked by Microstimulation in the Primate
1345 Superior Colliculus: Implications for Models of the SC Read-Out Process. *Frontiers in Integrative
1346 Neuroscience* 4. doi:10.3389/fnint.2010.00130
- 1347 Gurney, K., Prescott, T. J., and Redgrave, P. (2001a). A computational model of action selection in the
1348 basal ganglia. I. A new functional anatomy. *Biological cybernetics* 84, 401–10
- 1349 Gurney, K., Prescott, T. J., and Redgrave, P. (2001b). A computational model of action selection in the
1350 basal ganglia. II. Analysis and simulation of behaviour. *Biological cybernetics* 84, 411–23
- 1351 Hallworth, N. E., Wilson, C. J., and Bevan, M. D. (2003). Apamin-sensitive small conductance calcium-
1352 activated potassium channels, through their selective coupling to voltage-gated calcium channels, are
1353 critical determinants of the precision, pace, and pattern of action potential generation in rat subthalamic
1354 nucleus neurons in vitro. *The Journal of neuroscience* 23, 7525–7542
- 1355 Harsing, L. G. and Zigmond, M. J. (1997). Influence of dopamine on GABA release in striatum: evidence
1356 for D1-D2 interactions and non-synaptic influences. *Neuroscience* 77, 419–29
- 1357 Hazy, T. E., Frank, M. J., and O'Reilly, R. C. (2007). Towards an executive without a homunculus:
1358 computational models of the prefrontal cortex/basal ganglia system. *Philosophical Transactions of the
1359 Royal Society B: Biological Sciences* 362, 1601–1613. doi:10.1098/rstb.2007.2055
- 1360 Helms, M. C., Özen, G., and Hall, W. C. (2004). Organization of the Intermediate Gray Layer of the
1361 Superior Colliculus. I. Intrinsic Vertical Connections. *Journal of Neurophysiology* 91, 1706–1715.
1362 doi:10.1152/jn.00705.2003
- 1363 Hepp, K. and Henn, V. (1983). Spatio-temporal recoding of rapid eye movement signals in the monkey
1364 paramedian pontine reticular formation (PPRF). *Experimental brain research* 52, 105–120
- 1365 Hepp, K., Van Opstal, A. J., Straumann, D., Hess, B. J., and Henn, V. (1993). Monkey superior colliculus
1366 represents rapid eye movements in a two-dimensional motor map. *Journal of neurophysiology* 69,
1367 965–979
- 1368 Hernández-López, S., Bargas, J., Surmeier, D. J., Reyes, A., and Galarraga, E. (1997). D1 receptor
1369 activation enhances evoked discharge in neostriatal medium spiny neurons by modulating an L-type
1370 Ca²⁺ conductance. *The Journal of neuroscience : the official journal of the Society for Neuroscience* 17,
1371 3334–42
- 1372 Herrero, L., Corvisier, J., Hardy and, O., and Torres, B. (1998). Influence of the tectal zone on the
1373 distribution of synaptic boutons in the brainstem of goldfish. *The Journal of Comparative Neurology*
1374 401, 411–428. doi:10.1002/(SICI)1096-9861(19981123)401:3<411::AID-CNE8>3.0.CO;2-2
- 1375 Hikosaka, O., Takikawa, Y., and Kawagoe, R. (2000). Role of the basal ganglia in the control of purposive
1376 saccadic eye movements. *Physiological reviews* 80, 953–978
- 1377 Hikosaka, O. and Wurtz, R. H. (1983). Visual and oculomotor functions of monkey substantia nigra
1378 pars reticulata. IV. Relation of substantia nigra to superior colliculus. *Journal of neurophysiology* 49,
1379 1285–301
- 1380 Howard, L. A. and Tipper, S. (1997). Hand deviations away from visual cues: indirect evidence for
1381 inhibition. *Experimental brain research* 113, 144–152
- 1382 Humphries, M. D. and Gurney, K. N. (2002). The role of intra-thalamic and thalamocortical circuits in
1383 action selection. *Network: Computation in Neural Systems* 13, 131–156

- 1384 INCF Task Force on Multi-Scale Modeling (2011). Network Interchange for Neuroscience Modeling
1385 Language (NineML)
- 1386 Isa, T. (2002). Intrinsic processing in the mammalian superior colliculus. *Current Opinion in Neurobiology*
1387 12, 668–677. doi:10.1016/S0959-4388(02)00387-2
- 1388 Isa, T. and Hall, W. C. (2009). Exploring the Superior Colliculus In Vitro. *Journal of Neurophysiology*
1389 102, 2581–2593. doi:10.1152/jn.00498.2009
- 1390 James, S., Bell, O. A., Nazli, M. A. M., Pearce, R. E., Spencer, J., Tyrrell, K., et al. (2017). Target-distractor
1391 synchrony affects performance in a novel motor task for studying action selection. *PLOS ONE* 12,
1392 e0176945. doi:10.1371/journal.pone.0176945
- 1393 Jayaraman, A., Batton, R. R., and Carpenter, M. B. (1977). Nigrotectal projections in the monkey: an
1394 autoradiographic study. *Brain research* 135, 147–152
- 1395 Jiang, H., Stein, B. E., and McHaffie, J. G. (2003). Opposing basal ganglia processes shape midbrain
1396 visuomotor activity bilaterally. *Nature* 423, 982–986. doi:10.1038/nature01698
- 1397 Kaneda, K., Phongphanphanee, P., Katoh, T., Isa, K., Yanagawa, Y., Obata, K., et al. (2008). Regulation of
1398 Burst Activity through Presynaptic and Postsynaptic GABAB Receptors in Mouse Superior Colliculus.
1399 *Journal of Neuroscience* 28, 816–827. doi:10.1523/JNEUROSCI.4666-07.2008
- 1400 Kita, H. and Kitai, S. T. (1991). Intracellular study of rat globus pallidus neurons: membrane properties
1401 and responses to neostriatal, subthalamic and nigral stimulation. *Brain research* 564, 296–305
- 1402 Kleine, J. F. (2003). Saccade-Related Neurons in the Primate Fastigial Nucleus: What Do They Encode?
1403 *Journal of Neurophysiology* 90, 3137–3154. doi:10.1152/jn.00021.2003
- 1404 Knips, G., Zibner, S. K. U., Reimann, H., and Schöner, G. (2017). A Neural Dynamic Architecture for
1405 Reaching and Grasping Integrates Perception and Movement Generation and Enables On-Line Updating.
1406 *Frontiers in Neurorobotics* 11. doi:10.3389/fnbot.2017.00009
- 1407 Kühn, A. A., Williams, D., Kupsch, A., Limousin, P., Hariz, M., Schneider, G.-H., et al. (2004). Event-
1408 related beta desynchronization in human subthalamic nucleus correlates with motor performance. *Brain*
1409 : a journal of neurology 127, 735–46. doi:10.1093/brain/awh106
- 1410 Latto, R. (1977). The effects of bilateral frontal eye-field, posterior parietal or superior collicular lesions
1411 on brightness thresholds in the rhesus monkey. *Neuropsychologia* 15, 507–516
- 1412 Lee, C., Rohrer, W. H., and Sparks, D. L. (1988). Population coding of saccadic eye movements by neurons
1413 in the superior colliculus. *Nature* 332, 357–360. doi:10.1038/332357a0
- 1414 Lefèvre, P., Quaia, C., and Optican, L. M. (1998). Distributed model of control of saccades by superior
1415 colliculus and cerebellum. *Neural Networks* 11, 1175–1190
- 1416 Linden, R. and Perry, V. (1983). Massive retinotectal projection in rats. *Brain research* 272, 145–149
- 1417 Ling, L., Fuchs, A. F., Siebold, C., and Dean, P. (2007). Effects of initial eye position on saccade-related
1418 behavior of abducens nucleus neurons in the primate. *Journal of Neurophysiology* 98, 3581–3599
- 1419 Lynch, J. C., Hoover, J. E., and Strick, P. L. (1994). Input to the primate frontal eye field from the substantia
1420 nigra, superior colliculus, and dentate nucleus demonstrated by transneuronal transport. *Experimental*
1421 *Brain Research* 100, 181–186
- 1422 Maes, P. (1989). *The dynamics of action selection* (Artificial Intelligence Laboratory, Vrije Universiteit
1423 Brussel)
- 1424 Marcos, E. and Genovesio, A. (2016). Determining Monkey Free Choice Long before the Choice Is Made:
1425 The Principal Role of Prefrontal Neurons Involved in Both Decision and Motor Processes. *Frontiers in*
1426 *Neural Circuits* 10. doi:10.3389/fncir.2016.00075

- 1427 Marino, R. A., Trappenberg, T. P., Dorris, M., and Munoz, D. P. (2012). Spatial Interactions in the Superior
1428 Colliculus Predict Saccade Behavior in a Neural Field Model. *Journal of Cognitive Neuroscience* 24,
1429 315–336. doi:10.1162/jocn_a_00139
- 1430 Massone, L. L. E. (1994). A neural-network system for control of eye movements: basic mechanisms.
1431 *Biological Cybernetics* 71, 293–305. doi:10.1007/BF00239617
- 1432 Mays, L. E. and Sparks, D. L. (1980). Dissociation of visual and saccade-related responses in superior
1433 colliculus neurons. *Journal of Neurophysiology* 43, 207–232
- 1434 McCarthy, M. M., Moore-Kochlacs, C., Gu, X., Boyden, E. S., Han, X., and Kopell, N. (2011). Striatal
1435 origin of the pathologic beta oscillations in Parkinson's disease. *Proceedings of the National Academy
1436 of Sciences* 108, 11620–11625. doi:10.1073/pnas.1107748108
- 1437 McFarland, N. R. and Haber, S. N. (2002). Thalamic relay nuclei of the basal ganglia form both reciprocal
1438 and nonreciprocal cortical connections, linking multiple frontal cortical areas. *Journal of Neuroscience*
1439 22, 8117–8132
- 1440 McIlwain, J. T. (1982). Lateral spread of neural excitation during microstimulation in intermediate gray
1441 layer of cat's superior colliculus. *Journal of Neurophysiology* 47, 167–178
- 1442 McPeek, R. M. (2006). Incomplete Suppression of Distractor-Related Activity in the Frontal Eye Field
1443 Results in Curved Saccades. *Journal of Neurophysiology* 96, 2699–2711. doi:10.1152/jn.00564.2006
- 1444 McPeek, R. M., Han, J. H., and Keller, E. L. (2003). Competition Between Saccade Goals in the Superior
1445 Colliculus Produces Saccade Curvature. *Journal of Neurophysiology* 89, 2577–2590. doi:10.1152/jn.
1446 00657.2002
- 1447 McPeek, R. M. and Keller, E. L. (2002). Saccade Target Selection in the Superior Colliculus During a
1448 Visual Search Task. *Journal of Neurophysiology* 88, 2019–2034
- 1449 Meredith, M. A. and Ramoa, A. S. (1998). Intrinsic Circuitry of the Superior Colliculus: Pharmacophysio-
1450 logical Identification of Horizontally Oriented Inhibitory Interneurons. *Journal of Neurophysiology* 79,
1451 1597–1602
- 1452 Middleton, F. A. and Strick, P. L. (2000). Basal ganglia and cerebellar loops: motor and cognitive circuits.
1453 *Brain Research Reviews* 31, 236–250. doi:10.1016/S0165-0173(99)00040-5
- 1454 Mink, J. W. (1996). The basal ganglia: Focused selection and inhibition of competing motor programs.
1455 *Progress in Neurobiology* 50, 381–425
- 1456 Mink, J. W. and Thach, W. T. (1993). Basal ganglia intrinsic circuits and their role in behavior. *Current
1457 opinion in Neurobiology* 3, 950–957
- 1458 Mitchinson, B., Chan, T.-S., Chambers, J., Pearson, M., Humphries, M., Fox, C., et al. (2010). BRAHMS:
1459 Novel middleware for integrated systems computation. *Advanced Engineering Informatics* 24, 49–61.
1460 doi:10.1016/j.aei.2009.08.002
- 1461 Mitchinson, B. and James, S. S. (2015). BRAHMS. RRID: SCR_015642
- 1462 Monosov, I. E., Trageser, J. C., and Thompson, K. G. (2008). Measurements of simultaneously recorded
1463 spiking activity and local field potentials suggest that spatial selection emerges in the frontal eye field.
1464 *Neuron* 57, 614–625
- 1465 Morén, J., Shibata, T., and Doya, K. (2013). The Mechanism of Saccade Motor Pattern Generation
1466 Investigated by a Large-Scale Spiking Neuron Model of the Superior Colliculus. *PLoS ONE* 8, e57134.
1467 doi:10.1371/journal.pone.0057134
- 1468 Moschovakis, A. K., Kitama, T., Dalezios, Y., Petit, J., Brandi, A. M., and Grantyn, A. A. (1998). An
1469 Anatomical Substrate for the Spatiotemporal Transformation. *Journal of Neuroscience* 18, 10219–10229
- 1470 Munoz, D. P. (2002). Commentary: Saccadic eye movements: overview of neural circuitry. In *Progress in
1471 Brain Research*, ed. D. M. J. Hyona, W. Heide and R. Radach (Elsevier), vol. Volume 140. 89–96

- 1472 Munoz, D. P. and Everling, S. (2004). Look away: the anti-saccade task and the voluntary control of eye
1473 movement. *Nature Reviews Neuroscience* 5, 218–228. doi:10.1038/nrn1345
- 1474 Munoz, D. P. and Istvan, P. J. (1998). Lateral inhibitory interactions in the intermediate layers of the
1475 monkey superior colliculus. *Journal of Neurophysiology* 79, 1193–1209
- 1476 Nambu, A., Yoshida, S.-i., and Jinnai, K. (1990). Discharge patterns of pallidal neurons with input from
1477 various cortical areas during movement in the monkey. *Brain Research* 519, 183–191. doi:10.1016/
1478 0006-8993(90)90076-N
- 1479 N'Guyen, S., Thurat, C., and Girard, B. (2014). Saccade learning with concurrent cortical and subcortical
1480 basal ganglia loops. *Frontiers in Computational Neuroscience* 8. doi:10.3389/fncom.2014.00048
- 1481 Nishikawa, K., Biewener, A. A., Aerts, P., Ahn, A. N., Chiel, H. J., Daley, M. A., et al. (2007). Neurome-
1482 chanics: an integrative approach for understanding motor control. *Integrative and Comparative Biology*
1483 47, 16–54. doi:10.1093/icb/icm024
- 1484 Norman, D. A. and Shallice, T. (1986). Attention to action. In *Consciousness and self-regulation* (Springer).
1485 1–18
- 1486 Nowotny, T. (2011). Flexible neuronal network simulation framework using code generation for NVidia®
1487 CUDA™. *BMC Neuroscience* 12, P239. doi:10.1186/1471-2202-12-S1-P239
- 1488 Nowotny, T., Cope, A. J., Yavuz, E., Stimberg, M., Goodman, D. F., Marshall, J., et al. (2014). SpineML
1489 and Brian 2.0 interfaces for using GPU enhanced Neuronal Networks (GeNN). *BMC Neuroscience* 15,
1490 P148. doi:10.1186/1471-2202-15-S1-P148
- 1491 Olivier, E., Corvisier, J., Pauluis, Q., and Hardy, O. (2000). Evidence for glutamatergic tectotectal neurons
1492 in the cat superior colliculus: a comparison with GABAergic tectotectal neurons. *European Journal of
1493 Neuroscience* 12, 2354–2366
- 1494 Ottes, F. P., Van Gisbergen, J. A., and Eggermont, J. J. (1986). Visuomotor fields of the superior colliculus:
1495 A quantitative model. *Vision Research* 26, 857–873. doi:10.1016/0042-6989(86)90144-6
- 1496 OHalloran, A., OMalley, F., and McHugh, P. (2008). A review on dielectric elastomer actuators, technology,
1497 applications, and challenges. *Journal of Applied Physics* 104, 071101. doi:10.1063/1.2981642
- 1498 Papapavlou, C. and Moustakas, K. (2014). Physics-based modelling and animation of saccadic eye
1499 movement
- 1500 Parent, A. and Hazrati, L. (1993). Anatomical aspects of information processing in primate basal ganglia.
1501 *Trends in Neuroscience* 16, 111–116
- 1502 Pearson, K., Ekeberg, Ö, and Büschges, A. (2006). Assessing sensory function in locomotor systems using
1503 neuro-mechanical simulations. *Trends in Neurosciences* 29, 625–631. doi:10.1016/j.tins.2006.08.007
- 1504 Pearson, M. J., Pipe, A. G., Melhuish, C., Mitchinson, B., and Prescott, T. J. (2007). Whiskerbot: A robotic
1505 active touch system modeled on the rat whisker sensory system. *Adaptive Behaviour* 15
- 1506 Quaia, C., Lefèvre, P., and Optican, L. M. (1999). Model of the Control of Saccades by Superior Colliculus
1507 and Cerebellum. *Journal of Neurophysiology* 82, 999
- 1508 Quaia, C., Paré, M., Wurtz, R. H., and Optican, L. M. (2000). Extent of compensation for varia-
1509 tions in monkey saccadic eye movements. *Experimental Brain Research* 132, 39–51. doi:10.1007/
1510 s002219900324
- 1511 Redgrave, P., Prescott, T. J., and Gurney, K. (1999). The basal ganglia: a vertebrate solution to the selection
1512 problem? *Neuroscience* 89, 1009–1023
- 1513 Reppert, T. R., Lempert, K. M., Glimcher, P. W., and Shadmehr, R. (2015). Modulation of Saccade
1514 Vigor during Value-Based Decision Making. *Journal of Neuroscience* 35, 15369–15378. doi:10.1523/
1515 JNEUROSCI.2621-15.2015

- 1516 Reulen, J. P. H. (1984). Latency of visually evoked saccadic eye movements. *Biological Cybernetics* 50,
1517 251–262. doi:10.1007/BF00337075
- 1518 Richmond, P. (2015). DAMSON
- 1519 Richmond, P., Cope, A., Gurney, K., and Allerton, D. J. (2014). From Model Specification to Simulation
1520 of Biologically Constrained Networks of Spiking Neurons. *Neuroinformatics* 12, 307–323. doi:10.1007/
1521 s12021-013-9208-z
- 1522 Robinson, D. (1972). Eye movements evoked by collicular stimulation in the alert monkey. *Vision Research*
1523 12, 1795–1808. doi:10.1016/0042-6989(72)90070-3
- 1524 Robinson, D. A. (1975). Oculomotor control signals. In *Basic mechanisms of ocular motility and their
1525 clinical implications*, eds. G. Lennerstrand and P. Bach-y Rita (Oxford: Pergamon). 337–374
- 1526 Robinson, D. A. and Fuchs, A. F. (1969). Eye movements evoked by stimulation of frontal eye fields.
1527 *Journal of Neurophysiology* 32, 637–648
- 1528 Rovamo, J. and Virsu, V. (1979). An estimation and application of the human cortical magnification factor.
1529 *Experimental Brain Research* 37, 495–510. doi:10.1007/BF00236819
- 1530 Sabes, P. N., Breznen, B., and Andersen, R. A. (2002). Parietal representation of object-based saccades.
1531 *Journal of Neurophysiology* 88, 1815–1829
- 1532 Saint-Cyr, J. A., Ungerleider, L. G., and Desimone, R. (1990). Organization of visual cortical inputs to the
1533 striatum and subsequent outputs to the pallidonigral complex in the monkey. *Journal of Comparative
1534 Neurology* 298, 129–156
- 1535 Schall, J. D., Hanes, D. P., Thompson, K. G., and King, D. J. (1995). Saccade target selection in frontal
1536 eye field of macaque .1. Visual and premovement activation. *Journal of Neuroscience* 15, 6905–6918
- 1537 Schall, J. D. and Thompson, K. G. (1999). Neural selection and control of visually guided eye movements.
1538 *Annual review of neuroscience* 22, 241–259
- 1539 Schiller, P. H., Sandell, J. H., and Maunsell, J. H. (1987). The effect of frontal eye field and superior
1540 colliculus lesions on saccadic latencies in the rhesus monkey. *Journal of Neurophysiology* 57, 1033
- 1541 Schlag, J. D. (2002). Neurons that program what to do and in what order. *Neuron* 34, 177–178
- 1542 Schwartz, E. L. (1977). Spatial mapping in the primate sensory projection: Analytic structure and relevance
1543 to perception. *Biological Cybernetics* 25, 181–194. doi:10.1007/BF01885636
- 1544 Schwartz, E. L. (1980). Computational anatomy and functional architecture of striate cortex: A spatial
1545 mapping approach to perceptual coding. *Vision Res.* 20, 645–669
- 1546 Schweighofer, N., Arbib, M. A., and Dominey, P. F. (1996). A model of the cerebellum in adaptive control
1547 of saccadic gain. *Biological Cybernetics* 75, 19–28
- 1548 Scudder, C. A. (1988). A new local feedback model of the saccadic burst generator. *J Neurophysiol* 59,
1549 1454
- 1550 Segraves, M. A. and Goldberg, M. E. (1987). Functional properties of corticotectal neurons in the monkey's
1551 frontal eye field. *Journal of Neurophysiology* 58, 1387–1419
- 1552 Seth, A., Sherman, M., Reinbolt, J. a., and Delp, S. L. (2011). OpenSim: a musculoskeletal modeling
1553 and simulation framework for in silico investigations and exchange. *Procedia IUTAM* 2, 212–232.
1554 doi:10.1016/j.piutam.2011.04.021
- 1555 Slotnick, S. D., Klein, S. A., Carney, T., and Sutter, E. E. (2001). Electrophysiological estimate of human
1556 cortical magnification. *Clinical Neurophysiology* 112, 1349–1356
- 1557 Sommer, M. A. and Wurtz, R. H. (2000). Composition and topographic organization of signals sent from
1558 the frontal eye field to the superior colliculus. *Journal of Neurophysiology* 83, 1979–2001

- 1559 Sooksawate, T., Isa, K., Behan, M., Yanagawa, Y., and Isa, T. (2011). Organization of GABAergic
1560 inhibition in the motor output layer of the superior colliculus. *European Journal of Neuroscience* 33,
1561 421–432. doi:10.1111/j.1460-9568.2010.07535.x
- 1562 Sparks, D. L. (2002). The brainstem control of saccadic eye movements. *Nature Reviews Neuroscience* 3,
1563 952–964. doi:10.1038/nrn986
- 1564 Sparks, D. L. and Nelson, I. S. (1987). Sensory and motor maps in the mammalian superior colliculus.
1565 *Trends in Neurosciences* 10, 312–317. doi:10.1016/0166-2236(87)90085-3
- 1566 Stanton, G. B., Goldberg, M. E., and Bruce, C. J. (1988a). Frontal eye field efferents in the macaque
1567 monkey: I. Subcortical pathways and topography of striatal and thalamic terminal fields. *Journal of
1568 Comparative Neurology* 271, 473–492. doi:10.1002/cne.902710402
- 1569 Stanton, G. B., Goldberg, M. E., and Bruce, C. J. (1988b). Frontal eye field efferents in the macaque
1570 monkey: II. Topography of terminal fields in midbrain and pons. *The Journal of Comparative Neurology*
1571 271, 493–506. doi:10.1002/cne.902710403
- 1572 Sterling, P. (1971). Receptive fields and synaptic organization of the superficial gray layer of the cat
1573 superior colliculus. *Vision Research* 11, 309–IN47. doi:10.1016/0042-6989(71)90048-4
- 1574 Tabareau, N., Bennequin, D., Berthoz, A., Slotine, J.-J., and Girard, B. (2007). Geometry of the superior
1575 colliculus mapping and efficient oculomotor computation. *Biological cybernetics* 97, 279–292
- 1576 Takagi, M., Zee, D. S., and Tamargo, R. J. (1998). Effects of Lesions of the Oculomotor Vermis on Eye
1577 Movements in Primate: Saccades. *Journal of Neurophysiology* 80, 1911
- 1578 Talbot, S. and Marshall, W. (1941). Physiological Studies on Neural Mechanisms of Visual Localization
1579 and Discrimination*. *American Journal of Ophthalmology* 24, 1255–1264. doi:10.1016/S0002-9394(41)
1580 91363-6
- 1581 Tehovnik, E. J., Sommer, M. A., Chou, I.-H., Slocum, W. M., and Schiller, P. H. (2000). Eye fields in the
1582 frontal lobes of primates. *Brain Research Reviews* 32, 413–448. doi:10.1016/S0165-0173(99)00092-2
- 1583 Thelen, D. G. (2003). Adjustment of Muscle Mechanics Model Parameters to Simulate Dynamic
1584 Contractions in Older Adults. *Journal of Biomechanical Engineering* 125, 70. doi:10.1115/1.1531112
- 1585 Thivierge, J.-P. and Marcus, G. F. (2007). The topographic brain: from neural connectivity to cognition.
1586 *Trends in Neurosciences* 30, 251–259. doi:10.1016/j.tins.2007.04.004
- 1587 Thompson, K. G. and Bichot, N. P. (2005). A visual salience map in the primate frontal eye field. In
1588 *Progress in Brain Research*, eds. J. van Pelt, M. Kamermans, C. N. Levelt, A. van Ooyen, G. J. A.
1589 Ramakers, and P. R. Roelfsema (Elsevier), vol. 147 of *Development, Dynamics and Pathology of
1590 Neuronal Networks: from Molecules to Functional Circuits*. 249–262
- 1591 Thompson, K. G., Bichot, N. P., and Sato, T. R. (2005). Frontal eye field activity before visual search errors
1592 reveals the integration of bottom-up and top-down salience. *Journal of Neurophysiology* 93, 337–351
- 1593 Thurat, C., NGuyen, S., and Girard, B. (2015). Biomimetic race model of the loop between the superior
1594 colliculus and the basal ganglia: Subcortical selection of saccade targets. *Neural Networks* 67, 54–73.
1595 doi:10.1016/j.neunet.2015.02.004
- 1596 Tipper, S. P., Howard, L. A., and Paul, M. A. (2001). Reaching affects saccade trajectories. *Experimental
1597 Brain Research* 136, 241–249
- 1598 Ungerleider, L. G. and Mishkin, M. (1982). Two cortical visual systems. In *Analysis of Visual Behavior*,
1599 eds. D. J. Ingle, A. M. Goodale, and R. J. W. Mansfield (Cambridge, MA: MIT Press). 549–586
- 1600 Van Gisbergen, J., Van Opstal, A., and Tax, A. (1987). Collicular ensemble coding of saccades based on
1601 vector summation. *Neuroscience* 21, 541–555. doi:10.1016/0306-4522(87)90140-0
- 1602 Van Gisbergen, J. A. M., Van Opstal, A. J., and Schoenmakers, J. J. M. (1985). Experimental test of two
1603 models for the generation of oblique saccades. *Experimental brain research* 57, 321–336

- 1604 van Opstal, A. J. and Goossens, H. H. L. M. (2008). Linear ensemble-coding in midbrain superior colliculus
1605 specifies the saccade kinematics. *Biological Cybernetics* 98, 561–577. doi:10.1007/s00422-008-0219-z
- 1606 Van Opstal, A. J., Hepp, K., Hess, B. J., Straumann, D., and Henn, V. (1991). Two-rather than three-
1607 dimensional representation of saccades in monkey superior colliculus. *Science* 252, 1313–1315
- 1608 van Opstal, A. J. and van Gisbergen, J. A. (1990). Role of monkey superior colliculus in saccade averaging.
1609 *Experimental Brain Research* 79, 143–149
- 1610 Vokoun, C. R., Huang, X., Jackson, M. B., and Basso, M. A. (2014). Response Normalization in the
1611 Superficial Layers of the Superior Colliculus as a Possible Mechanism for Saccadic Averaging. *Journal*
1612 *of Neuroscience* 34, 7976–7987. doi:10.1523/JNEUROSCI.3022-13.2014
- 1613 Vokoun, C. R., Jackson, M. B., and Basso, M. A. (2010). Intralaminar and Interlaminar Activity within the
1614 Rodent Superior Colliculus Visualized with Voltage Imaging. *Journal of Neuroscience* 30, 10667–10682.
1615 doi:10.1523/JNEUROSCI.1387-10.2010
- 1616 Vokoun, C. R., Jackson, M. B., and Basso, M. A. (2011). Circuit dynamics of the superior colliculus
1617 revealed by in vitro voltage imaging: Vokoun et al. *Annals of the New York Academy of Sciences* 1233,
1618 41–47. doi:10.1111/j.1749-6632.2011.06166.x
- 1619 Waitzman, D. M., Ma, T. P., Optican, L. M., and Wurtz, R. H. (1991). Superior colliculus neurons mediate
1620 the dynamic characteristics of saccades. *Journal of Neurophysiology* 66, 1716–1737
- 1621 Walker, R., Deubel, H., Schneider, W. X., and Findlay, J. M. (1997). Effect of remote distractors on saccade
1622 programming: evidence for an extended fixation zone. *Journal of neurophysiology* 78, 1108–1119
- 1623 Wickens, J. (1997). Basal ganglia: structure and computations. *Network: Computation in Neural Systems*
1624 8, 77–109
- 1625 Wilson, C. and Kawaguchi, Y. (1996). The origins of the two-state spontaneous membrane potential
1626 fluctuations of neostriatal spiny neurons. *The Journal of Neuroscience* 16, 2397–2410
- 1627 Wilson, C. J. (2004). A Model of Reverse Spike Frequency Adaptation and Repetitive Firing of Subthalamic
1628 Nucleus Neurons. *Journal of Neurophysiology* 91, 1963–1980. doi:10.1152/jn.00924.2003
- 1629 Wilson, E. D., Assaf, T., Pearson, M. J., Rossiter, J. M., Anderson, S. R., Porrill, J., et al. (2016). Cerebellar-
1630 inspired algorithm for adaptive control of nonlinear dielectric elastomer-based artificial muscle. *Journal*
1631 *of The Royal Society Interface* 13, 20160547. doi:10.1098/rsif.2016.0547
- 1632 Wu, H. H., Williams, C. V., and McLoon, S. C. (1994). Involvement of nitric oxide in the elimination
1633 of a transient retinotectal projection in development. *SCIENCE-NEW YORK THEN WASHINGTON-*,
1634 1593–1593
- 1635 Wurtz, R. H. and Albano, J. E. (1980). Visual-motor function of the primate superior colliculus. *Annual*
1636 *review of Neuroscience* 3, 189–226. doi:10.1146/annurev.ne.03.030180.001201
- 1637 Wurtz, R. H. and Goldberg, M. E. (1972). Activity of superior colliculus in behaving monkey. III. Cells
1638 discharging before eye movements. *J Neurophysiol* 35, 575–586
- 1639 Yu, J., Tan, M., Wang, S., and Chen, E. (2004). Development of a biomimetic robotic fish and its control
1640 algorithm. *IEEE Transactions on System, Man and Cybernetics - Part B* 34, 1798–1810

FIGURES

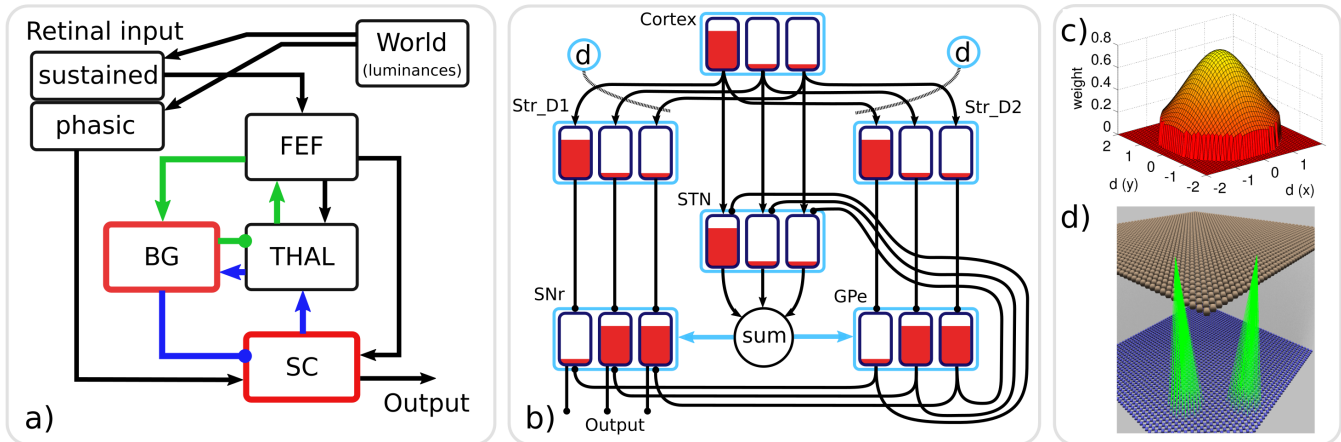


Figure 1. a) The macroscopic architecture of the Cope-Chambers model. The main nuclei modelled as brain systems are: basal ganglia (BG), frontal eye fields (FEF), thalamus (THAL) and superior colliculus (SC). The retinal input is presented via non-biologically accurate retinal populations. The loops through basal ganglia, which define the architecture, are shown with coloured lines: the cortical loop (through FEF and THAL) in green and the sub-cortical loop (through SC and THAL) in blue. Connections with arrowheads indicate excitatory connections, those with circles are inhibitory. A red border indicates that the box represents a sub-system of two or more populations; a black box indicates (at least, within the context of the model) a single neural population. The BG box is expanded in: **b) The basal ganglia model component.** This shows a basal ganglia comprising striatum (Str.D1 & Str.D2), subthalamic nucleus (STN), globus pallidum externum (GPe) and substantia nigra reticulata (SNr). The model has three action channels shown as black boxes within each blue population border. Three channels of cortical input to the BG are also depicted. Red indicates the activation level of a given channel, helping to illustrate the selection mechanism. For example, the channel indicated by the leftmost bar has a high salience (cortical input) and excites activity in Str.D1 which then inhibits the leftmost bar in SNr. The diffuse projection from STN is equivalent to summing its projections channel-wise, and then projecting the sum to all channels of its target populations (the blue arrows indicate that all channels of GPe and SNr are targeted by the connection). Dopaminergic modulation of the inputs to the striatum are indicated by the blue circles labelled ‘d’ and the dotted lines. The SNr sends inhibitory output projections to its targets. **c) 2D Gaussian weights.** The ‘GaussianKernel’ connectivity pattern is based on the in-plane component of the displacement between the location of a neural element in one layer, and the location of a target neural element in the target layer for the connection. The potential weight of the connection is given by a 2D Gaussian function, which is maximum for the target neuron which exactly corresponds to the source neuron, and drops down for target neurons which are horizontally displaced from the source neuron. A threshold is applied to avoid a computationally expensive all-to-all connectivity (with most of these connections having negligible weight values). If the weight is non-zero, then a connection is made from source to target, otherwise no connection is made. **d) Gaussian connectivity.** This image shows connectivity (green rays) from two source neurons (in Str.D2, brown spheres) to target neurons (in GPe, blue spheres). The circular connectivity pattern is seen. This does not show the weight *values*, which reduce ‘towards the edge of the circle’ and follow the relationship shown in (c).

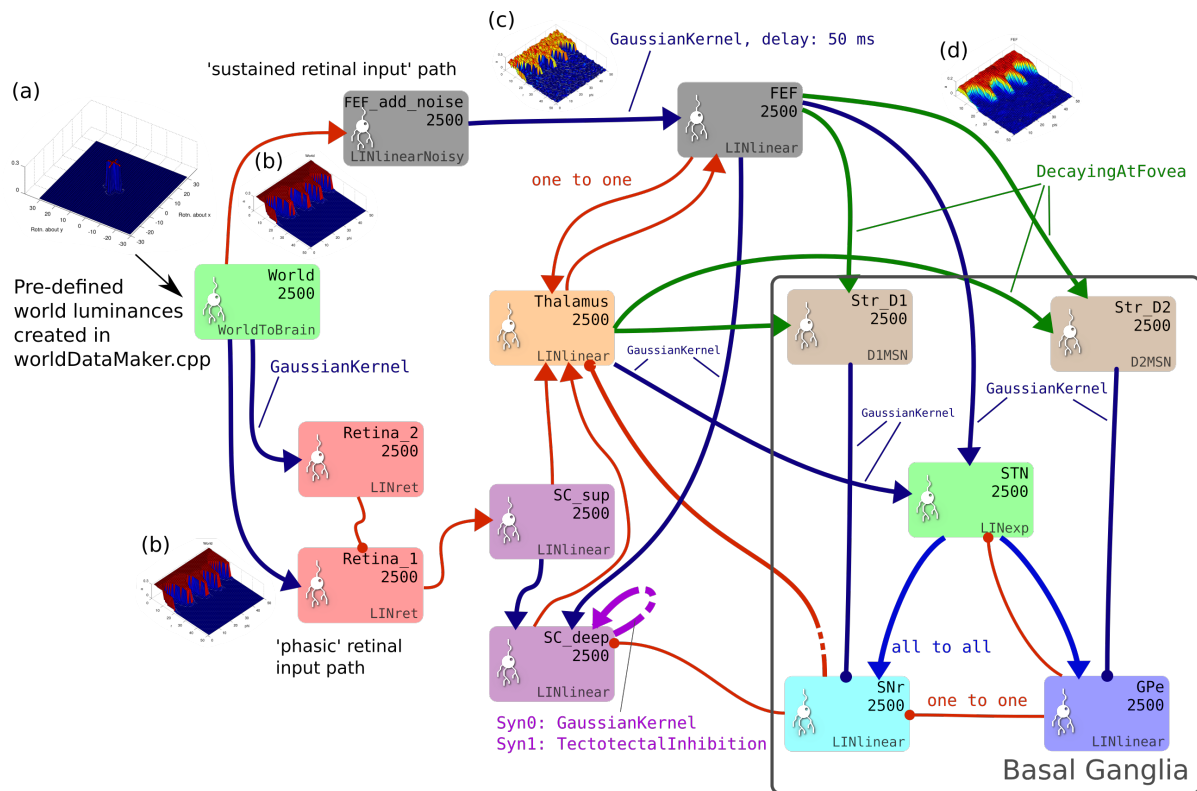


Figure 2. The brain model. This is the SpineCreator ‘network layer’ view of the model. Each box represents a neural population with 2500 elements, arranged in a 50×50 grid. The SpineML component name is printed on the bottom right corner of each population box and the population name is at the top. The overall connectivity between populations is represented by the projection arrows with the colour indicating the connectivity scheme (one-to-one connections are red, Gaussian kernel connections are dark blue and so on). Excitatory connections have arrowheads and inhibitory connections have circles, although for full details of the behaviour of the connections, the weight-update and post-synapse component associated with each connection must be referred to. Briefly, the model comprises a *World* population, into which a retinotopically organised view of the world is introduced. This information is passed into cortical populations (FEF) and subcortical populations (SC) via a simple model of the retina. These feed a cortico-thalamo-basal ganglia loop, which selects which region of the deep layer of superior colliculus should be disinhibited, allowing activity to build up therein. The five populations comprising the basal ganglia are enclosed in a grey outline. Note that substantia nigra pars compacta is not modelled here, instead the level of dopamine in the striatum is set via a parameter in the Str.D1 and Str.D2 populations. **a**) Fixation cross input in Cartesian eye frame. **b**) Fixation cross input in retinotopic co-ordinates. **c**) Fixation cross with noise added. **d**) After blurring, input is passed to BG populations.

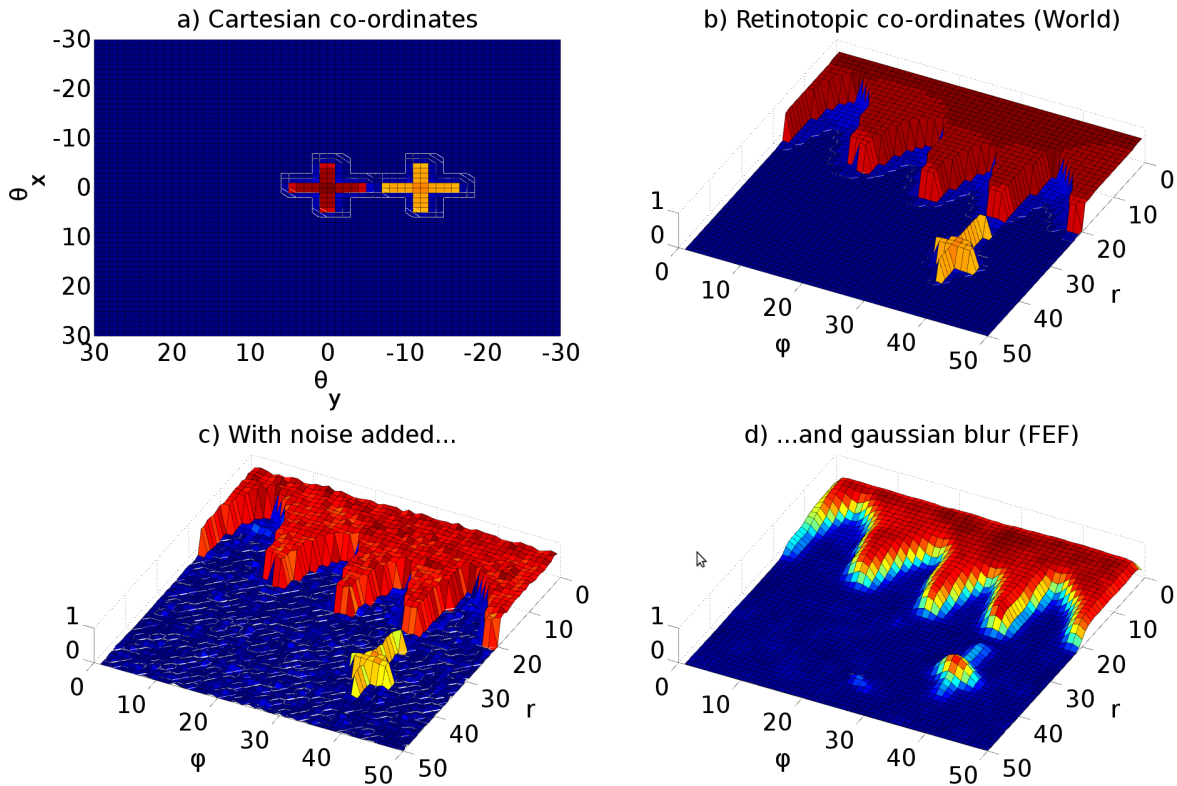


Figure 3. Representative mapping from eye's frame of reference in Cartesian co-ordinates to retinotopic co-ordinates. **a)** The mapping of luminances in the eye's frame of reference. The world input is pre-defined by a JSON configuration file. Luminance position, size and shape can be defined in this file, along with the times at which luminances appear and disappear. The `worldDataMaker.cpp` code computes the locations of the luminances in the eye's frame of reference, given its rotational state. It also computes a 2D Gaussian convolution of the luminances. Here, there are two cross shaped luminances spanning 10° , one of value 0.8 at the fixation point (0,0) and one of value 0.5 at a peripheral position ($0, -12^\circ$). Note that these crosses have the same ‘bar width’ of 2° as the crosses used in the simulations, but their span of 10° is greater than the 6° used in the simulations, to make these images clearer. **b)** The locations of the luminances in the eye's frame of reference are then converted into retinotopic co-ordinates, with centrally located luminances being represented at low values of r and more peripheral luminances having higher values of r . ϕ encodes rotational angle: 1 and 50 encode upward movement; 13.5 is left; 26 is down; 38.5 is right. The output of the World component is fed into `FEF_add_noise` and into the retinal neuron populations. The colour map makes it possible to distinguish between the two crosses. **c)** The `FEF_add_noise` populations adds a level of noise to the signal representing processing of the signal in visual cortex. **d)** A Gaussian projection from `FEF_add_noise` to `FEF` further blurs the activity in `FEF`. `FEF` is the input to the basal ganglia and one input to superior colliculus.

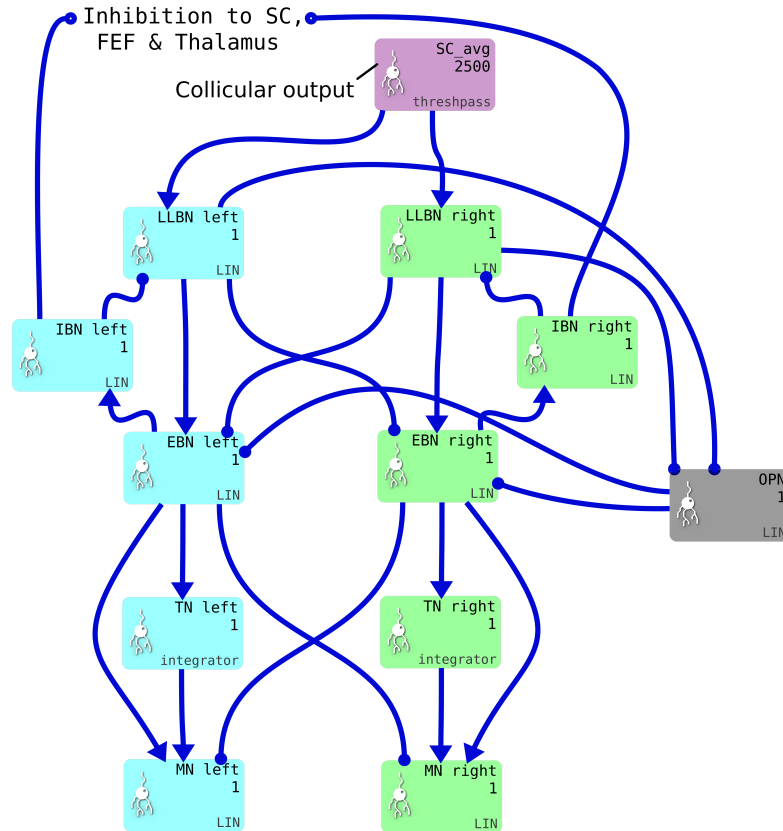


Figure 4. One pair of channels of the saccadic burst generator (SBG) for left (cyan) or right (green) movements. Collicular activity in SC_avg excites the channels via SBG weight maps, which are encoded as explicit lists of connection weights in the blue connection arrows from SC_avg to the LLBN populations. Each box represents a neural population and shows the population name, the number of neural elements (here 2500 or 1) and the SpineML component name; LIN for Leaky integrator or *integrator*. Key: LLBN: Long lead burst neurons; IBN: Inhibitory burst neurons; OPN: Omnipause neurons; EBN: Excitatory burst neurons; TN: Tonic neurons; MN: Motoneurons.

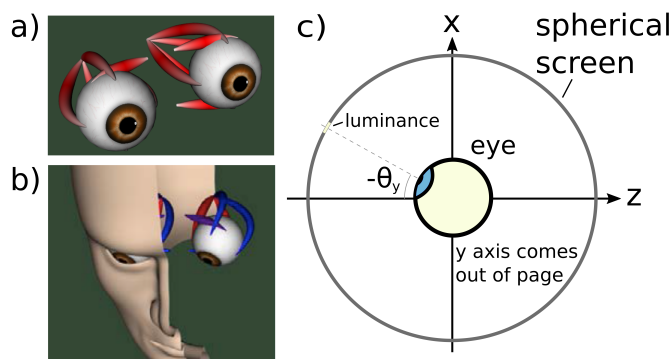


Figure 5. The biomechanical eye. **a)** an OpenSim rendering of a pair of biomechanical eyes showing the positions of the extraocular muscles. Note that i) volume visualization of muscles should not be confused with FEM muscle models; it is provided for user feedback purposes, i.e. shape and color change depending on the muscle activation, ii) superior and inferior oblique are visualized up to their respective muscle pulleys. **b)** OpenSim rendering of biomechanical eye within a head model **c)** Top-down schematic cross-sectional view of the biomechanical eye situated within a spherical screen, with a horizontal rotation towards a luminance at an angle of $-\theta_y$ about the *y* axis. The *y* axis points up, out of the page.

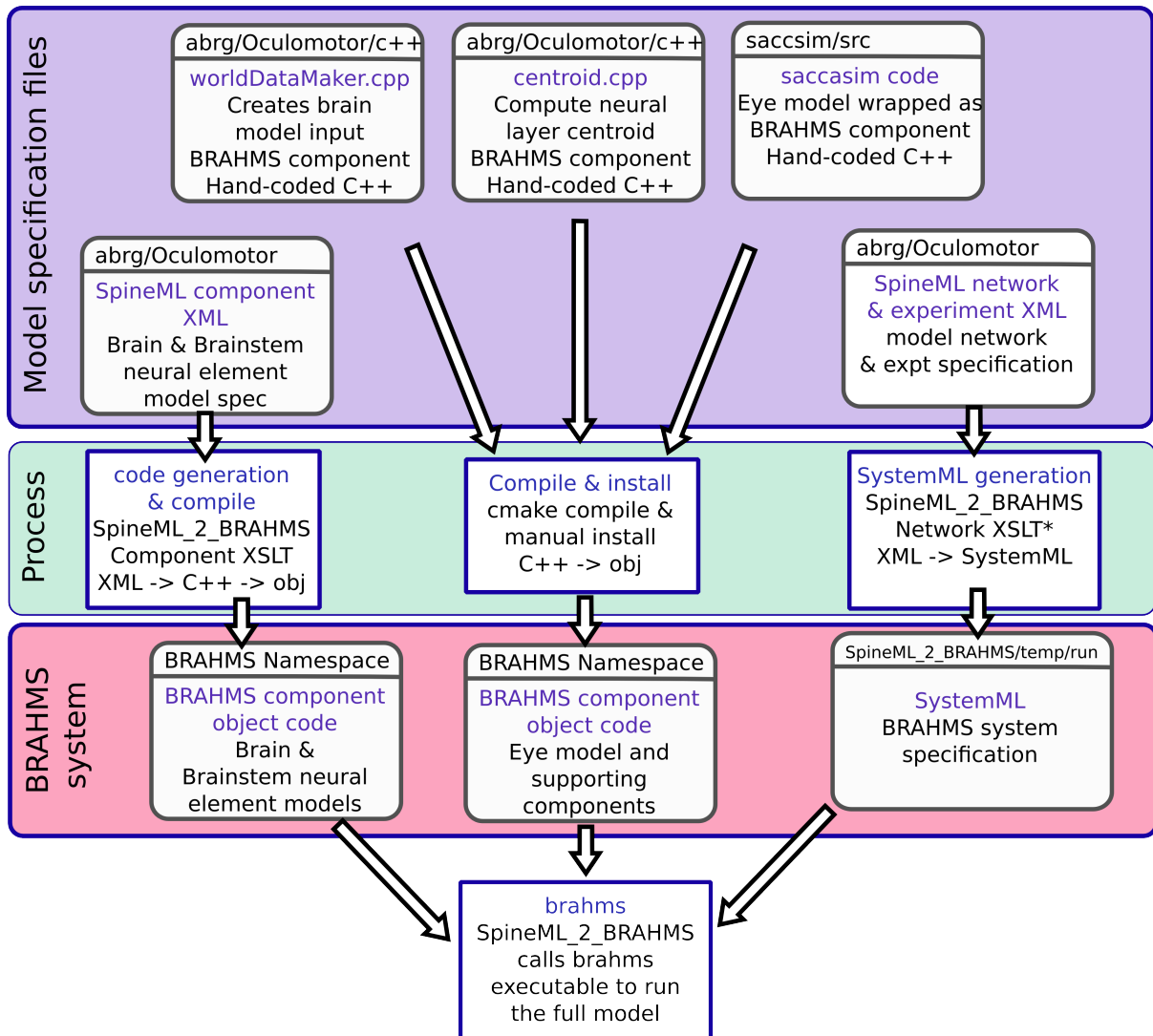


Figure 6. The model framework. **a)** The model is specified using a combination of declarative XML files and hand-coded C++. These original model specifications are shown within the blue box. **b)** The green box shows the processes which are applied to the model specification to produce the BRAHMS system. Most of the process is defined within the scripts which make up SpineML_2_BRAHMS, but the hand-written components must be manually compiled and installed within the BRAHMS Namespace, allowing the BRAHMS executable to locate them at runtime. **c)** The red box shows the resulting BRAHMS system ready to be executed by the BRAHMS executable. In practice, this call is made by SpineML_2_BRAHMS.

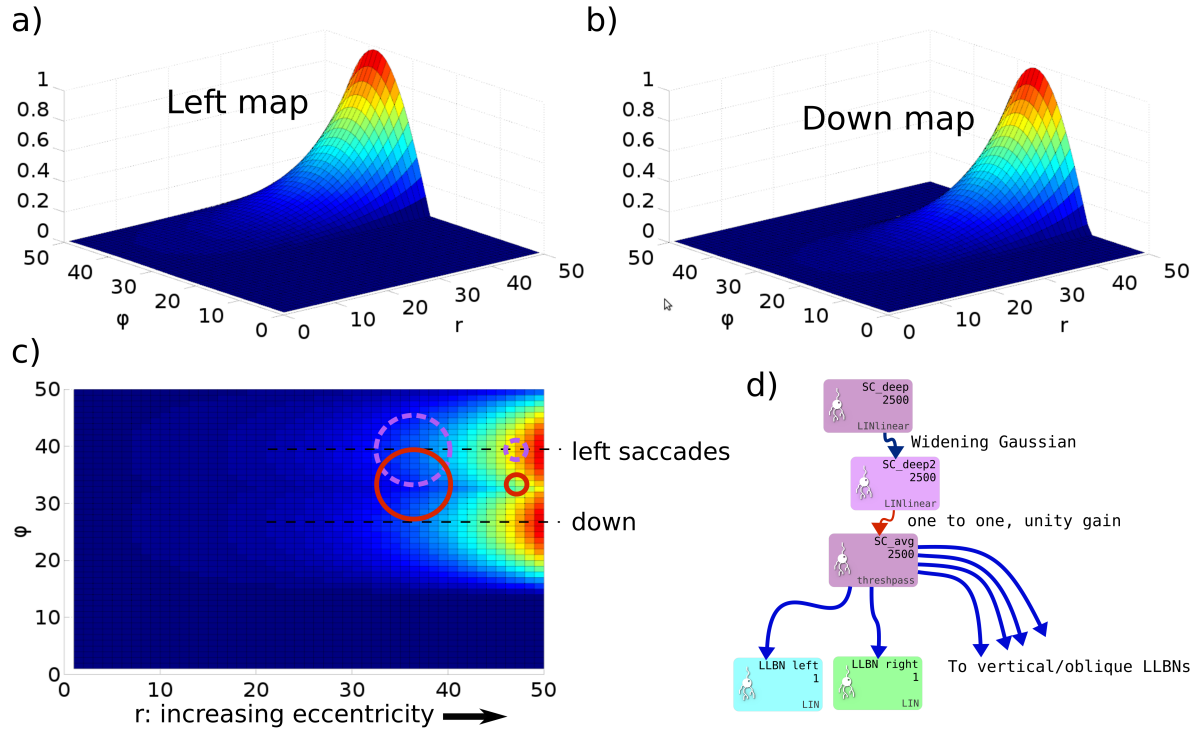


Figure 7. a) & b) Tabareau-style weight maps for 'left' and 'down' components of a saccade. c) The two weight maps in (a) and (b) shown on the same graph, viewed from above. Circles show the locations of potential hills of activity. Purple, dashed circles encode saccades left; red circles encode saccades with both a left and a down component. d) Showing the additional deep layer of superior colliculus (SC_deep2) and the output layer (SC_avg, named for the fact that in an earlier version of the model, it received the output of the centroid of SC_deep). The widening Gaussian projection is shown as the arrow between SC_deep and SC_deep2.

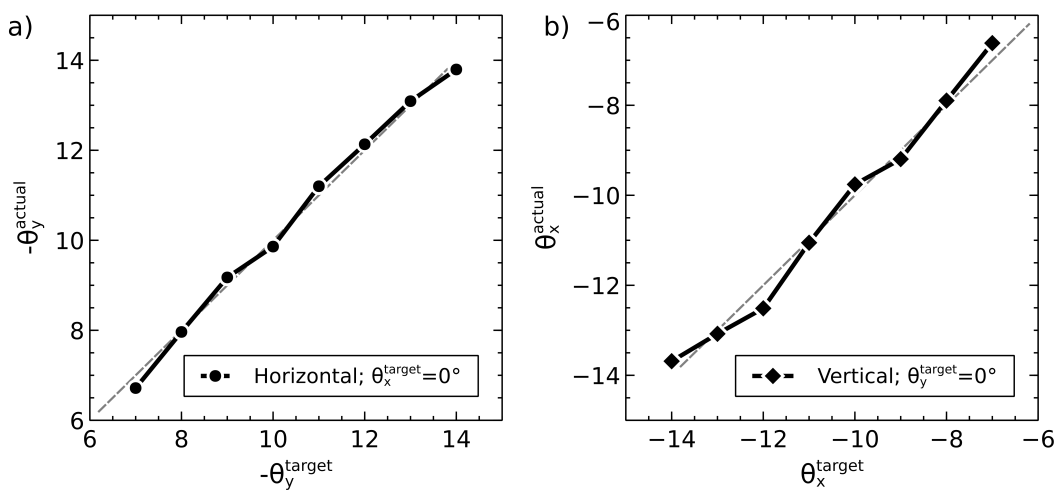


Figure 8. Accuracy of single saccades at different target eccentricities for fixation luminance 0.2 and target luminance 0.3. a) Horizontal rotations about the y axis. b) Vertical rotations of the eye about the x axis.

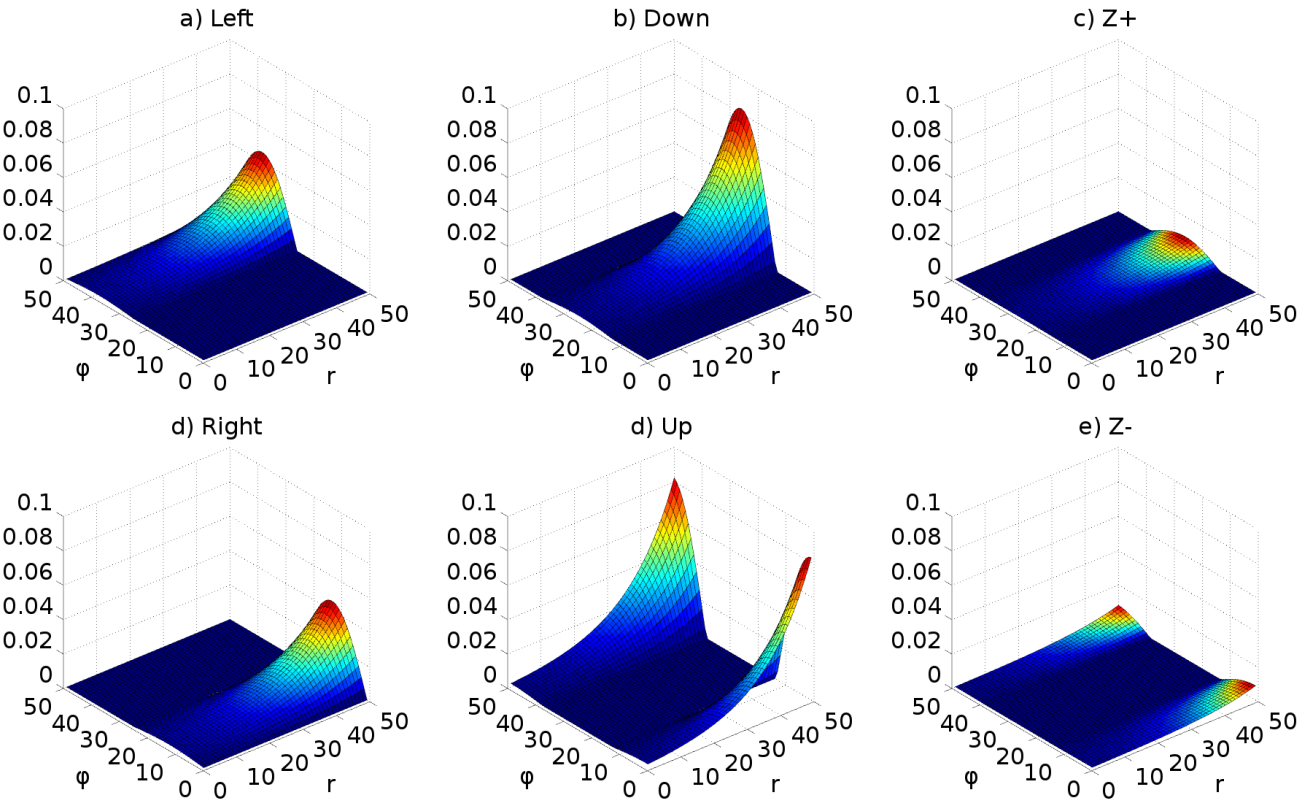


Figure 9. Weight maps for the connections between the output layer of superior colliculus and the six long lead burst neurons of the saccadic burst generator model. Each map increases exponentially with increasing r , multiplied by $\cosine(\phi)$ about its ‘active’ axis. **a)** Weight map for leftward movements which innervates the lateral rectus in this single left-eye model. **b)** Map for downward movements; innervates the inferior rectus. **c)** Superior oblique muscle weight map. **d)** Weight map for rightward movements/medial rectus muscle. **e)** Weight map for the superior rectus muscle which generates upward movements. **f)** Inferior oblique map.

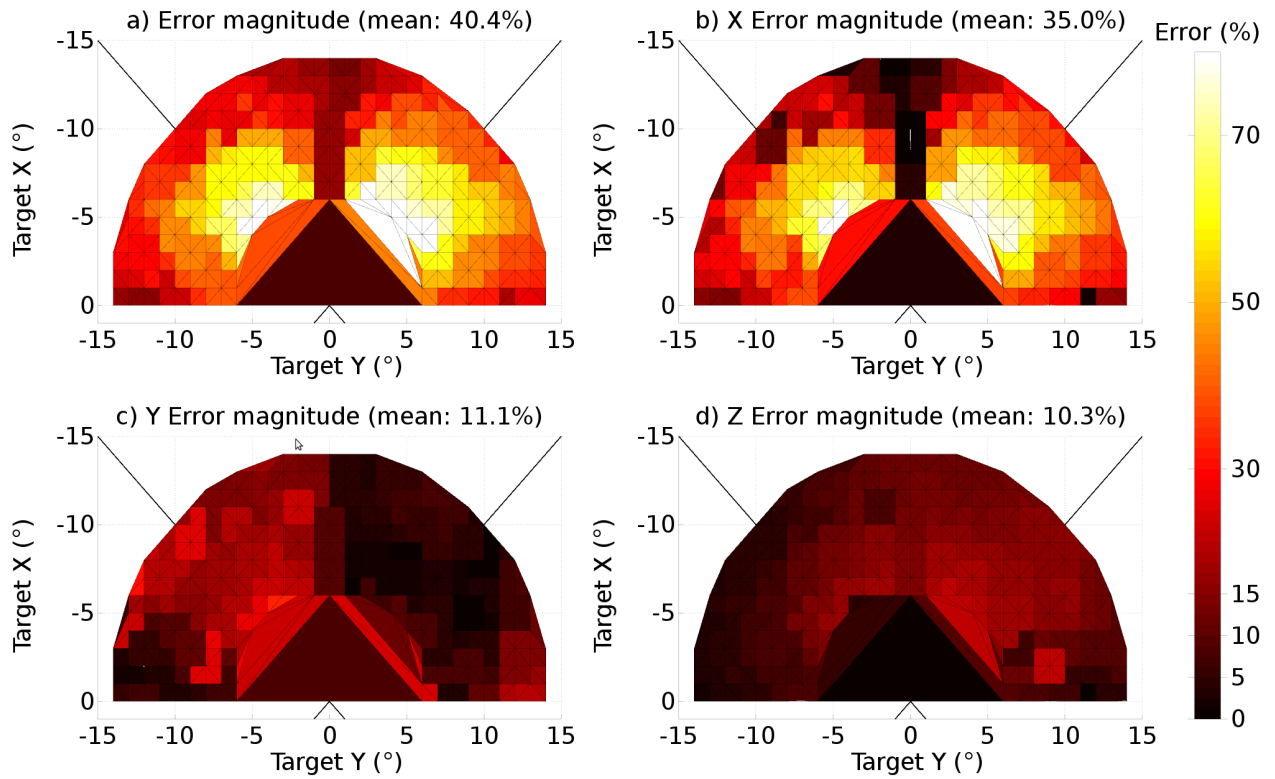


Figure 10. The end-point error surface for the original, naïve model (TModel3). **a)** The ratio of the magnitudes of the total error vector and the target vector, expressed as a percentage. **b)** The ratio of the magnitude of the x component of the error vector to the magnitude of the target vector, expressed as a percentage. **c)** As (b) but for the y component. **d)** As (b), for z component. All colour maps are shown with the same scale. The target rotations, θ_x^t and θ_y^t are denoted ‘Target X’ and ‘Target Y’ in the figure.

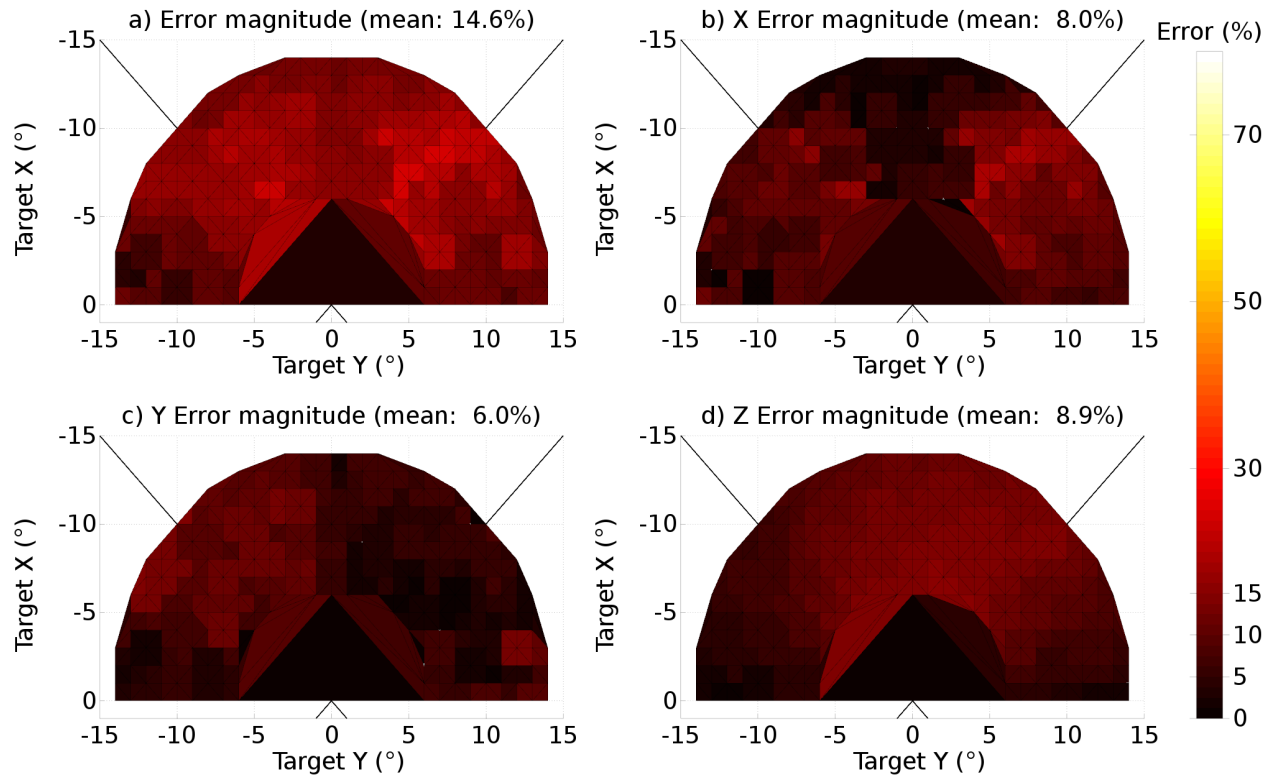


Figure 11. The end-point error surface for the model in which a widening projection field was added to the model of the superior colliculus. **a)** The ratio of the magnitudes of the total error vector and the target vector, expressed as a percentage. **b)** The ratio of the magnitude of the x component of the error vector to the magnitude of the target vector, expressed as a percentage. **c)** As (b) but for the y component. **d)** As (b), for z component. All colour maps are shown with the same scale. The target rotations, θ_x^t and θ_y^t are denoted ‘Target X’ and ‘Target Y’ in the figure. Note that the range of the colour scale is 0 to 20%, a much smaller range than in Fig 10.

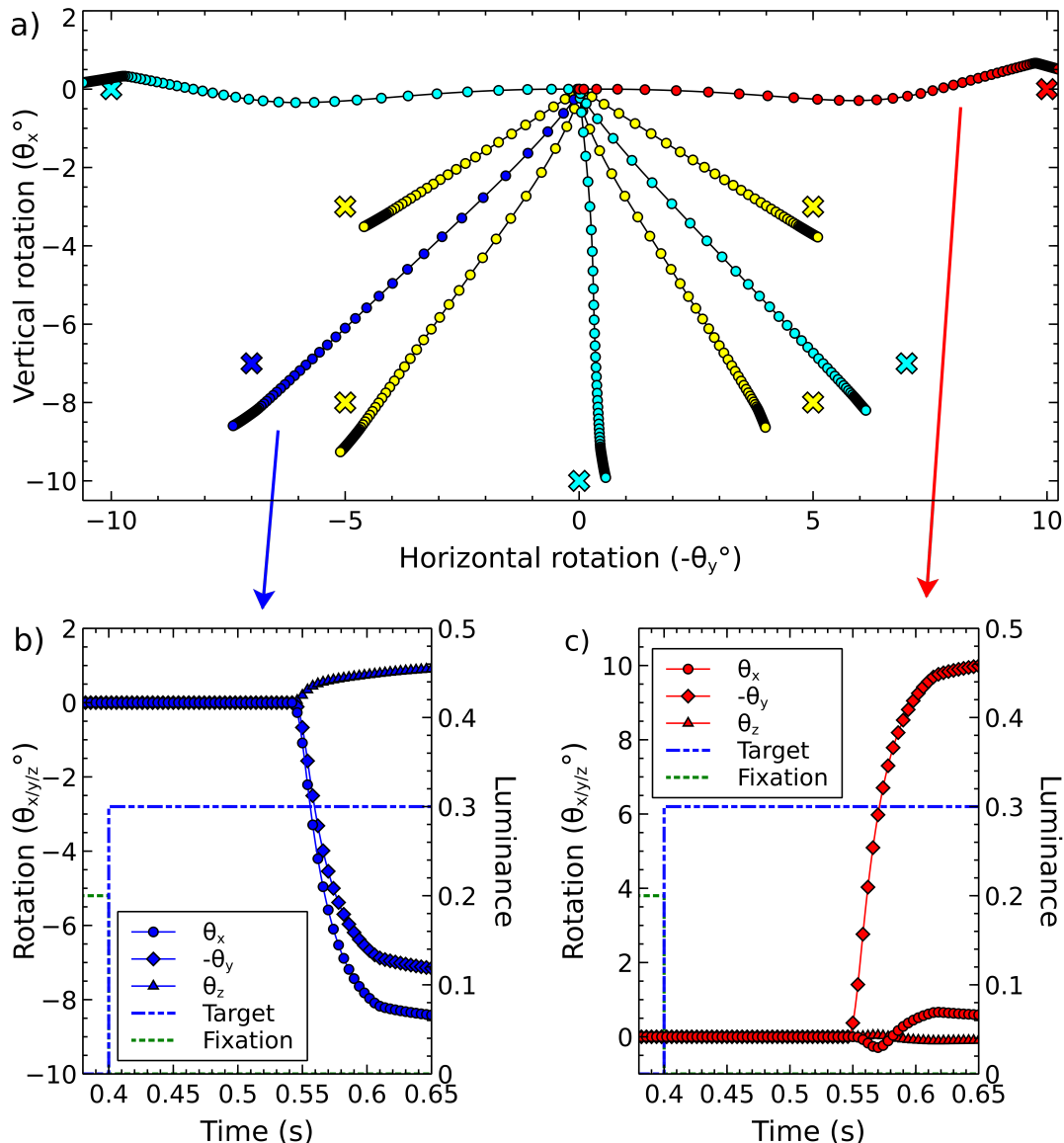


Figure 12. Representative single saccades. **a)** Trajectories from 9 saccades to a single target at 9 different locations. In each case, a fixation cross luminance of magnitude 0.2 was displayed at (0,0), the start position of the eye, until time 0.4 s. The target luminance, magnitude 0.3, was illuminated at time 0.4 s. Trajectory shape is dependent on the target position, and there is a variable amount of error in the end-points achieved by the model. Colour is used in this diagram as an aid to distinguishing different saccades and their targets; for a given saccade, the target location is given by the cross of the same colour closest to the end of the trajectory. **b)** The three rotational components of the ‘dark blue’ saccade, to target location (-7,-7). **c)** The three rotational components of the ‘red’ saccade, to target location (0,-10).

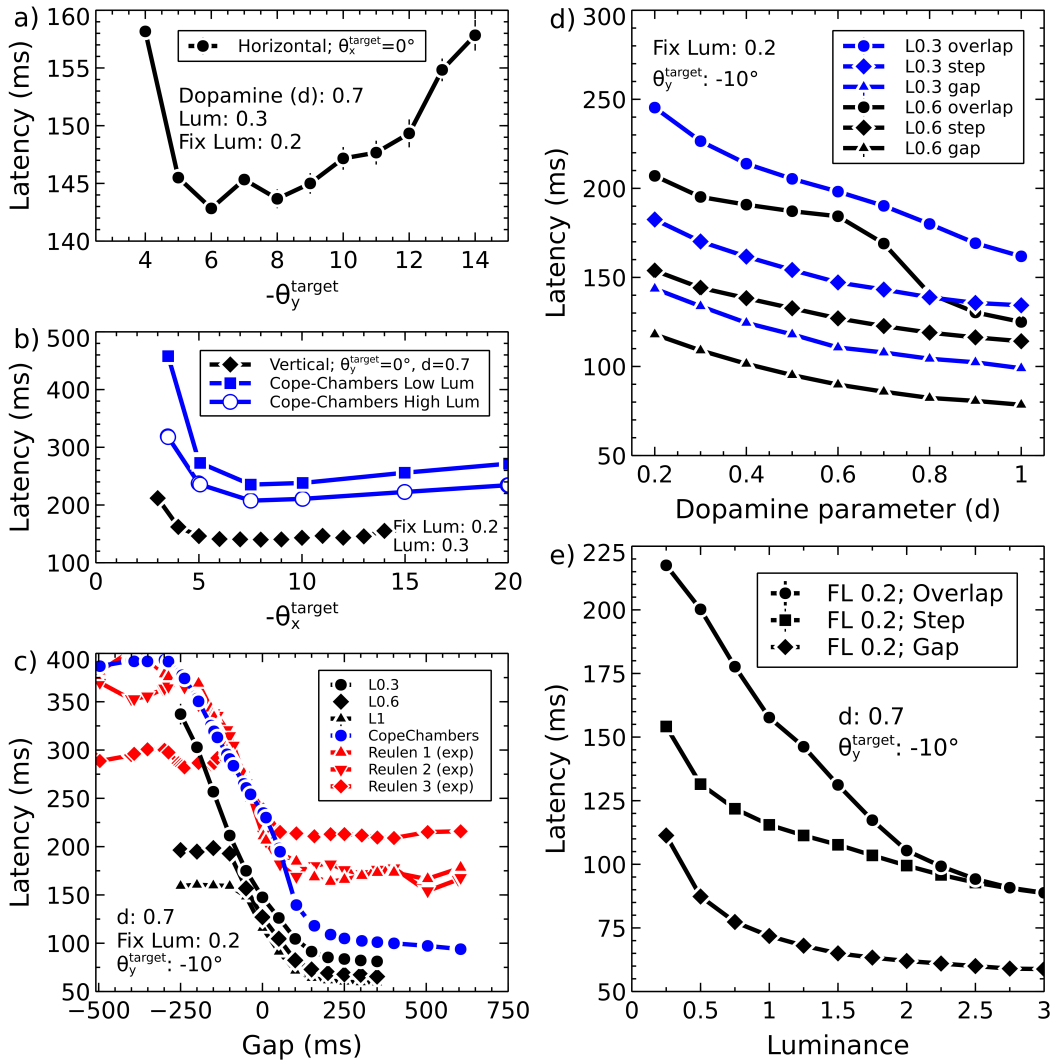


Figure 13. Exploring saccade latencies. **a)** Latency to first movement as a function of target eccentricity for horizontal targets. **b)** Latency vs. eccentricity for vertical targets. **c)** Latency vs. gap at three different luminance values. The data are shown alongside the Cope-Chambers model results from Fig. 5 of Cope et al. (2017) in blue, and the experimental results used in that model in red. The fixation luminance for the Cope-Chambers curve was 0.5, the target luminance 0.6 and the target eccentricity was 8° . The difference between the Cope-Chambers model data and the data from the current model results from the different mechanism by which activity in SC_deep causes a movement, the differing target angle and the reduced fixation luminance used here. **d)** The effect of the dopamine parameter on saccade latencies in gap, step and overlap conditions, for two different target luminances. **e)** Saccade vs. luminance showing gradual transition between reflexive and express behaviour.

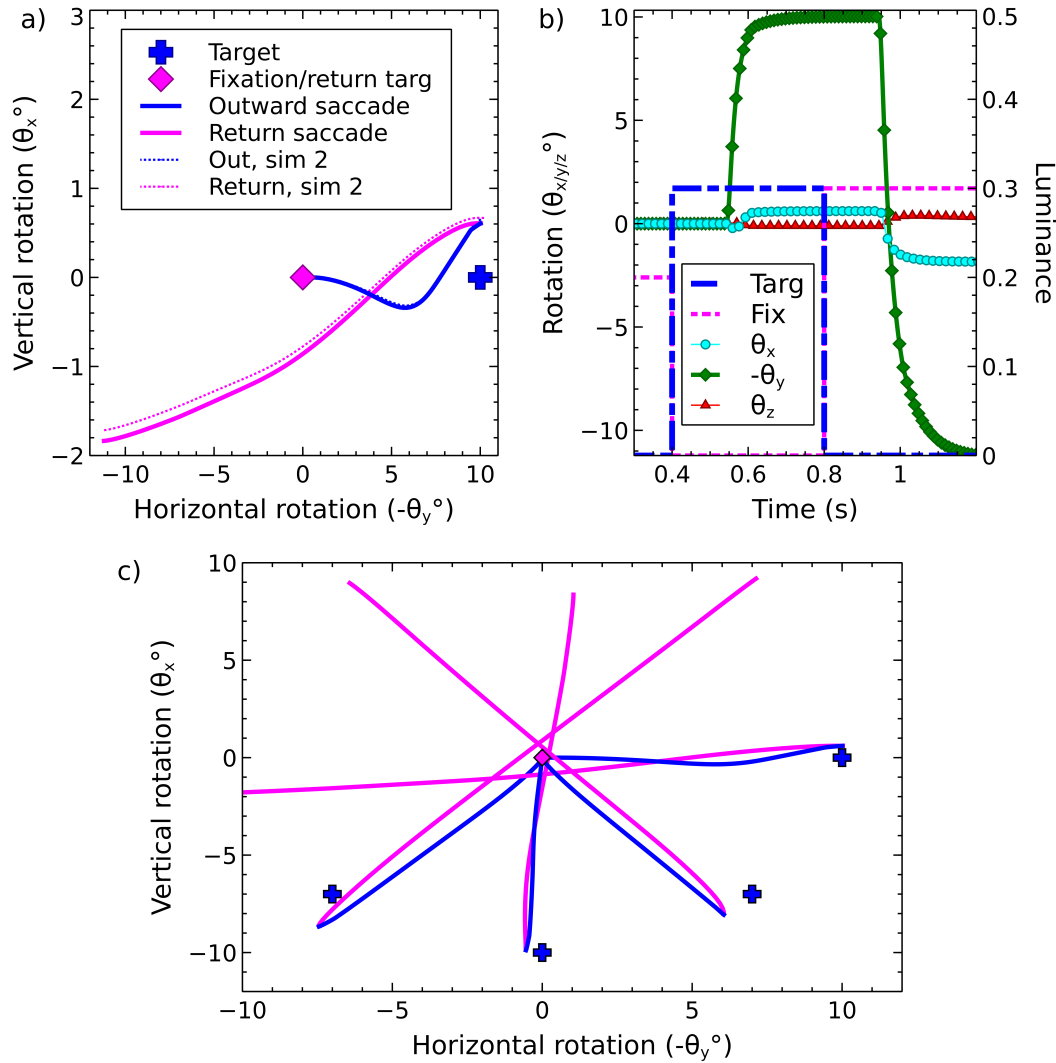


Figure 14. There and back - a saccade to a target, followed by return to the original fixation. **a)** Out and return saccade to a target at (0, -10°). The outward trajectory is shown in blue, the return in pink. **b)** Rotational components of the saccade shown in (a). **c)** Outward and return trajectories for the saccade shown in (a) alongside saccades to three other targets.

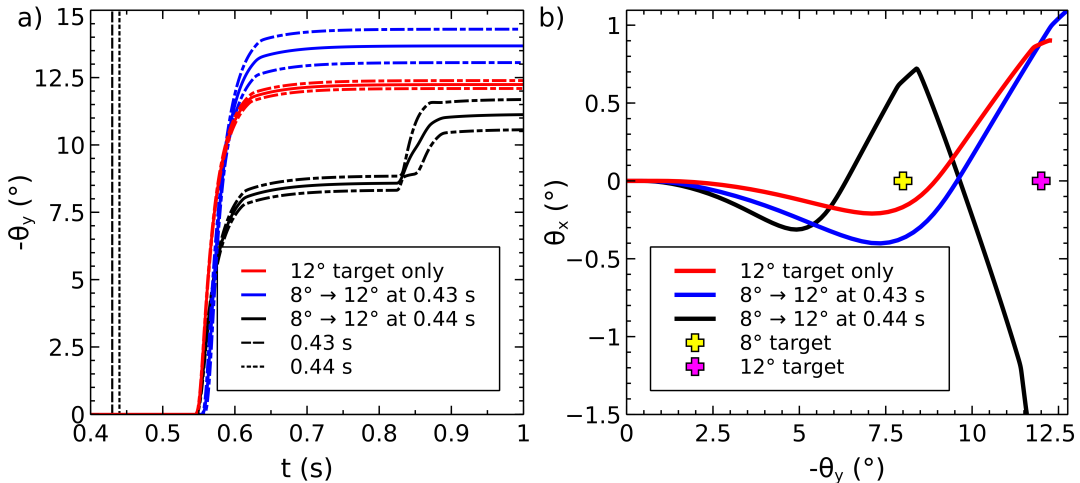


Figure 15. Double steps. The effect of illuminating a first target at 8° or 12° , followed by a second target at 12° or 8° . **a)** Horizontal rotation of the eye plotted vs. time for a saccade to the 12° target only (red), and to an 8° target at 0.4 s followed by a 12° target after 30 ms (blue) or 40 ms (black). The timings are indicated by vertical lines. When the second target is presented up to 30 ms after the initial target, the initial target has not had time to dominate the output saccade and a saccade to a location close to the second target is made. If the delay is 40 ms or more, the activity from the initial target has time to cause a built up of activity in SC_deep and an initial saccade close to the first target is made, followed, after a longer than usual latency period, with a second saccade closer to the second target. In this graph, the mean of five separate simulations is plotted along with ± 1 standard deviation around the mean. **b)** The θ_x/θ_y trajectories corresponding to the data presented in (a).